HERON is jointly edited by:
STEVIN-LABORATORY of the
faculty of Civil Engineering,
Delft University of Technology,
Delft, The Netherlands
and
TNO-INSTITUTE
FOR BUILDING MATERIALS
AND STRUCTURES.
Rijswijk (ZH), The Netherlands
HERON contains contributions
based mainly on research work
performed in these laboratories
on strength of materials, structures
and materials science.

ISSN 0046-7316

Secretary:
G. J. van Alphen
Stevinweg 1
P.O. Box 5048
2600 GA Delft, The Netherlands
Tel. 0031-15-785919
Telex 38070 BITHD

HERON vol. 34
1989
no. 3

Contents

REINFORCED CONCRETE BEAMS UNDER SHOCK LOADING, LINEAR AND NONLINEAR RESPONSE

A. G. T. J. Heinsbroek
Delft Hydraulics, P.O. Box 117, Delft

J. Blaauwendraad
Delft University of Technology, Delft

This publication has been issued in close co-operation with the Netherlands Technology Foundation (STW).

Publication in HERON since 1970

Notations

A	cross-sectional area
a	element length
B^e	interpolation matrix
c_b	longitudinal wave velocity
C	damping matrix
c_L	longitudinal wave velocity
c_R	Rayleigh wave velocity
c_s	transversal wave velocity
DLF	dynamic load factor
E	Young's modulus
E_c'	Young's modulus for concrete
E_s	Young's modulus for steel
EI	bending stiffness of the beam
e	spring deformation (elongation)
η	correction factor shear stress distribution
ε^e	strain vector
ε_g^e	generalised strain vector
F	concentrated load
F_p	plastic resistance force
f	distributed load
f_{ccm}	mean compressive strength concrete (NL)
f_{cm}	prismatic compressive strength concrete
f_{ctm}	mean tensile strength concrete
f_{cw}	mean compressive strength concrete (D)
f_{st}	tensile strength reinforcement steel
f_w	resistance force of the structure with regard to the load
$\hat{F}$	amplitude concentrated load
$\hat{f}$	amplitude distributed load
G	shear modulus: $G = E/2(1 + \nu)$
γ	shear
γ^2	integration coefficient
h	beam height
I	stress moment of inertia
i	impulse per unit length
J	element mass moment of inertia
$\boldsymbol{K}$	stiffness matrix
k	spring stiffness
$\boldsymbol{k}$	load vector
$\varkappa$	curvature
$\varkappa_{cr}$	curvature at which cracking begins
$\varkappa_{sy}$	curvature at which reinforcement steel yields

$\varkappa_u$	ultimate curvature at failure
l	length
λ	wave length
M	bending moment
M_{cr}	bending moment at which cracking begins
M_e	effective mass
M_p	full plastic bending moment
M_{sy}	bending moment at which reinforcement steel yields
M_u	ultimate bending moment at failure
$\boldsymbol{M}$	mass matrix
$\boldsymbol{M}^e$	element mass matrix
m	mass per unit length
μ	ductility demand
μ_u	ultimate ductility
ν	lateral contraction coefficient (Poisson's ratio)
ω, ω_n	eigenfrequency
ω_0	percentage of reinforcement at the bottom of a beam or a plate
ω_b	percentage of reinforcement at the top of a beam or a plate
Q	shear force
R	dynamic support reaction
ϱ	mass density
$\boldsymbol{\sigma}^e$	stress vector
$\boldsymbol{\sigma}_g^e$	generalised stress vector
T	natural period
t	time
t_a	starting point in time
t_d	positive phase length (duration)
t_{max}	point in time at which the maximum value is reached
t_r	rise time of a load
τ_d	relative positive phase length (t_d/T)
u	displacement, degree-of-freedom
$\boldsymbol{u}^e$	displacement field
V	volume
$\boldsymbol{v}, \boldsymbol{v}^e$	displacement vector
w_{max}	maximum deflection
w_{pla}	permanent deflection

Preface

This volume of Heron reports on the research of A. G. T. J. Heinsbroek for his Ph.D. thesis, carried out under the supervision of J. Blaauwendraad, Professor of Civil Engineering at Delft University of Technology. Here only a selection of the thesis work is presented.
In this thesis research, extensive use has been made of a newly developed computer program called TILLY. This program will not be described in too much detail. A future volume of Heron is planned to be devoted to this software tool for structural mechanics.
It is worthwhile to mention that the main development was done in a PC environment.
The project was completely financed by the Netherlands Technology Foundation (STW). The translation into English by Anneke Visser, Delft.

Reinforced concrete beams under shock loading, linear and nonlinear response

1 Definition of the problem

In everyday life structures are regularly damaged in explosions and may even collapse as a result of either directly exerted overpressure or by flying fragments. Not only explosions during storage or transport of dangerous substances such as oil and gas (LNG, LPG, etc) are thought of, but also explosions that, under certain conditions, may occur in many seemingly ordinary substances (e.g. milk powder, flour). Many accidents are also caused by collisions, falling objects, etc.

The often large, suddenly imposed loads, may lead to considerable stress in the structure, which may cause cracking, plastic yielding and subsequently collapse. In this respect, designing and supervising authorities are facing a problem, about which many questions are still unanswered. Practice is specially interested in the resilience, the permanent deformation and the damage that together determine the criteria for the assessment of the behaviour of a structure.

The behaviour of a structure is determined by: the nature and the magnitude of the load, the type of structure (beam, portal, plate, shell, etc), the size of the structure and the material used (steel, reinforced concrete, pre-stressed concrete, timber, plastic). The type of structure determines the nature of the support behaviour: via strain (extension), bending, shear, torsion, etc.

With a given type of material the size of the structure determines the strength as well as its stiffness and its mass.

Much is already known regarding the response to specified dynamic loads on structures in the elastic stage, that is to say, for global computations. A lot of experience has been gained with computations in which the structure and the load are schematically condensed into a simple mass-spring system. Examples can be found in the books of Biggs [1] and Baker [2]. The opinion has been established that this simple system may lead to a good approximation of displacements and occurring bending moments. However, there are reasons to mistrust the shear forces computed in this way, certainly with strongly impulsive loads.

But there is another aspect. The loads resulting from explosions are usually so heavy that the behaviour will have to be examined far beyond the elastic stage. Therefore, material properties such as cracking of concrete and plastic yielding of steel, play an important role in the behaviour. For example, with beams and plates of reinforced concrete, the quality of the concrete and the percentage of reinforcement will be of great influence and this leads to the question which models of computation are justified. In this study attention is restricted to beams of reinforced concrete.

As is generally known, so-called full plastic hinges, which can transfer a constant plastic moment, may develop in a beam loaded under certain conditions. When a shear force

has also to be transferred in this cross-section, the magnitude of the maximum transferable plastic moment decreases. Now problems arise, firstly, because a suddenly imposed load may cause strong shear forces to develop and secondly, because shear forces and bending moments vary rapidly with time. Thus different combinations are continually found at different positions. Another complication is that, even when a bending moment causes a full plastic hinge to develop so that the structure shows ductile behaviour, brittle collapse may occur due to shear force. This means that previously ductile behaviour of a structure may suddenly be thwarted or the ductile behaviour of one of the components in the system may not be developed at all. Also the fact that material properties change due to rapid deformations is a complication and a relatively uncertain factor. Furthermore, in collisions with a local character, the load on the structure and the behaviour of the structure as a whole are also determined by the deformation, and possibly the collapse, of the material that was hit directly and the material in the adjacent areas.

1.1 *Objective*

Considering the previous paragraph, the most general objective of the project can be described as follows. The response is determined within both the elastic and the plastic domain, given the required physical and geometrical parameters with regard to both the structure and the load. A designer needs criteria concerning damage and collapse. In this study the extent of damage is an objective (in the form of plastic rotations). Conclusions concerning the acceptability of the damage are beyond the aim of this research. It is only predicted to what extent the structure is damaged due to dynamic load.
This objective has been described in terms stemming from the physical "reality". However, this reality is too complicated to be fully described in mechanical and mathematical models. This concerns the schematic representation of the structure, of the load and of the limit states of the structure, and the determination of the response resulting from these three schematic representations.
An additional problem is the wide variety of structural forms. In actual practice, beams and plates occur over one or more spans in seemingly random proportions and sizes. More complicated structural forms are also possible. It has been decided not to involve the structural form into the research as a variable. Here, only a simple structure, a simply supported beam, will be taken into consideration. The type of support is not determined in advance and also the type of loading and the loading rate will be varied. Using the description and restrictions mentioned above as a framework, the objective of this study may be formulated as follows.
Determine the exact response of a simply supported beam, subjected to a suddenly imposed load, varying several parameters. These parameters are : support conditions, geometrical load distribution and development in time of the load, the latter being divided into the time function and a time that characterizes the duration of the load.
The eventual objective of this study is to supply designers with data concerning the way in which dynamically loaded structures have to be modelled. The research results have

to show under which conditions the usual approach with simple mass-spring models can be used, and in which cases this will not be sufficient, and of course, what then the approach ought to be.
Previously, in Heron volume 28, 1983, no. 1, Blaauwendraad and Van der Veen published an article on similar computations. However, they discussed one special case and by hook and by crook used a program that had not been developed for that objective. Now a program is used that has been geared to the problem and the very objective is to gain general insight in a wide category of cases.

1.2 *Parameters*

The three parameters: support, geometrical load distribution and development in time of the load are varied as follows. The two supports of the beam are either "simply supported" or "clamped" (Dutch: "Vrij opgelegd" or "Ingeklemd"). This is denoted by the letters V and I respectively. The uniformly distributed load and the concentrated load (Dutch: "Gelijkmatig verdeeld" and "Puntlast"), denoted by G and P, were taken for the load distribution over the length of the beam. The distribution with time of the load can be varied according to the form of the time function and to a characteristic rate parameter.
Two types of triangular load are taken for the form of the time function: the explosion load (or shock wave load) and the collision load (Dutch: "Botsing") (see Fig. 1). These are denoted by the letters E and B.

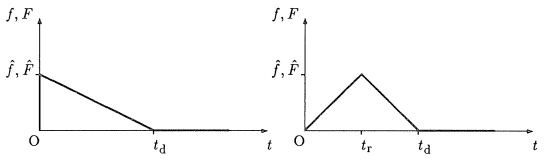

Explosion (triangular load) — Collision load (symmetrical triangular load)

Fig. 1. Explosion load and collision load.

The first is also called triangular load and exists of a jump of the load at point in time 0, followed by a linear decrease with time after which at point in time t_d the load is back to zero and remains so. The duration t_d is called positive phase length. The collision load, also called symmetrical triangular load, consists of a linear increasing load during interval 0 to t_r and a linear decreasing load during interval t_r to t_d. The load is zero at point in time 0, maximal at point in time t_r and again zero starting from point in time t_d. The symmetry of this load is expressed by:

$$t_r = 0.5 t_d \tag{1}$$

As far as the concentrated load is concerned, it has to be stated that triangular load is not considered, as this combination is less relevant for the practice. A concentrated load

is a typical result of a fragment colliding with the beam, whereas a triangular load is associated with a shock wave. Also the clamped support is left out of the consideration of the concentrated load, which is motivated by the fact that the characteristic difference between a concentrated load and a uniformly distributed load is to be found in the middle of the span and not in the support. For it is on the edge of the load zone that the perturbation develops, in the form of shear forces and bending moments, which will propagate in waves through the beam.
The variation in the loading rate is expressed by the relation of t_d and T, in which T is the eigenperiod of the fundamental tone of the beam, hereafter to be called the fundamental period. This relation is called the relative positive phase length, denoted by τ_d.
The various combinations are identified with the help of 4 parameters, see Table 1. The categories 1 to 5 inclusive, denote a relative positive phase length τ_d of 10.0, 1.00. 0.50, 0.10 and 0.01 respectively.

Table 1. Identification of the parameters from which the combinations are made

support	load development in time	load distribution with space	loading rate
V	E	G	1-5
I	B	P	inclusive

A specific computation is denoted by a combination of letters and a digit. So VEG3 means: simply supported beam under a uniformly distributed explosion load, with a relative positive phase length of 0.50. The combinations discussed in this study are (apart from the loading rate) VEG, IEG, VBG, IBG and VBP.

1.3 *Method*

To determine the exact response of a simply supported beam to a transient load, several methods are available. These methods can be classified in accordance with the schematic representation of the structure and the mathematical description of this scheme. This study does not include the possible mathematical solutions that are generally available. In Chapter 3, however, the mathematical solution, which has been implemented in the computer program used in this study, is mentioned.

Continuous systems
The schematic representation can be subdivided into continuous and discrete systems. Continuous systems may either be one, two or three dimensional, in which physical and geometrical properties are attributed to infinitesimal line elements, area elements or volume elements respectively. Examples of one-dimensional schematic representations are the Bernoulli-Euler beam, the Rayleigh beam, the shear-bending beam and the Timoshenko beam. In each of these schematic representations the beam is thought

to be a system line, with every point on that line having properties describing the stiffness and inertial properties of the cross-section of the beam at that point.
Continuous methods generally give a very accurate description of local and rapidly varying phenomena. The restrictions of the modelling, however, are an important disadvantage. For example, in the case of dynamically responding plates, the differential equations can only be solved for a limited number of boundary conditions. Also allowing for plastic properties soon leads to unsolvable equations.
From studies on continuous modelling it can be concluded which quantities are relevant, to determine the response of beams to explosion loads as accurately as possible. Already in 1914, Lamb [3] indicated that the simple Bernoulli-Euler beam, which only shows bending deformation and translation inertia, displays an infinitely high propagation velocity with suddenly imposed loads. In 1921, Timoshenko [4] suggested to extend the Bernoulli-Euler theory with the rotation inertia as indicated by Rayleigh as well as with a possibility for shear deformation, as had already been applied with deep beams under static loading conditions. In 1942, Flügge proved that a suddenly imposed elastic perturbation indeed moved through the Timoshenko beam at a finite propagation speed. A more detailed description of the application of this Timoshenko theory can be found in the graduation project of Leussink [5]. Heinsbroek showed that the influence of the rotation inertia is relatively unimportant [6].
Therefore, a suitable model requires at least the following quantities: bending deformation, shear deformation, translation inertia and, to a lesser degree, rotation inertia. Also the velocity of various types of wave propagation can be derived from continuous schematic representations. This matter will be elaborated upon in Chapter 2.
In this study the continuous methods will also be used, to check the concurrence of the response resulting from computations with the discrete element method, with the response resulting from the continuous models.

Discrete systems
In discrete schematic representations the deflected shape of the beam is determined by a finite number of degrees-of-freedom. Internal stress resultants, external load forces and inertial forces are exerted on these degrees-of-freedom. As there is no initial stress due to imperfections and temperature differences, the stress resultants result from mutual displacements of the degrees-of-freedom. The inertial forces develop as a result of the acceleration of that specific degree-of-freedom (lumped mass), or as a result of the acceleration of other degrees-of-freedom (consistent mass). The load forces are autonomous and have been derived from concentrated loads, line loads, area loads and volume loads. Examples, ranged in accordance with increasing complexity are: the single mass-spring system, the multi-mass-spring system and the finite element method.
As stated before, the single mass-spring system is often used in practice. When the response resulting from dynamic loads closely resembles the first eigenmode, it can be adequately computed by using the single mass-spring system. Response computed with the help of a single mass-spring system is the product of a position function and a time

function. However, when the response consists of significantly higher eigenmodes, it will no longer be possible to describe it with the single mass-spring system. Higher eigenmodes may be caused by certain geometrical and/or time dependent properties of the load in relation to the collection of eigenmodes of the beam.
Also when the behaviour of the beam enters the plastic area, the response is no longer of constant shape with time. In that case it becomes very hard, if not impossible, to decide how the spring should be schematically represented, for in order to do this, the position of the yielding hinge or yielding hinges has to be known. Should this have been hypothetically decided, it will constantly have to be adjusted during the time of the response. Only in those cases in which the plastic response is characterized by the development of a dominant plastic hinge, e.g. in the middle of a simply supported beam, use of the single mass-spring system is justified.
Multi-mass-spring systems and finite element methods can be used to describe local and shifting phenomena. If the degrees-of-freedom are chosen well, it will be possible to describe the continuous real physical system with sufficient accuracy. The finite element method, on which computer programs such as DIANA, ANSYS, ADINA and others are based, has the advantage of being generally valid, and requiring only the constitutive model of the compounding materials. From this the properties of the cross-sections are made up at any point in time. So far, however, little experience has been gained on the combination of non-linear behaviour and time step processes in the finite element method. Because of the large number of elements and degrees-of-freedom, the required amount of computer memory is large and computing times are still long. The method is not yet suitable for a study in which many parameters have to be varied.
In this study the approach with a multi-mass-spring system will be called "discrete element method". For this approach a relatively small number of elements and degrees-of-freedom are required, but choosing the right spring properties assumes knowledge of the properties of the cross-section. These have now become input and will have to be derived from other research, if possible.
This method has been preferred in this study. Computing time is short and the required computer memory is small, so that a personal computer can be used, if necessary. Moreover, the TILLY program, which was initiated by Blaauwendraad, is available to actually carry out these computations [10], [25], [31], [32].
In the application of the discrete element method, both one-dimensional and multi-dimensional continua can be schematically represented. In a one-dimensional representation, the properties at the level of the cross-section of the beam are modelled into springs and if necessary into dash-pots in a certain geometrical order. In multi-dimensional circumstances, the properties can be schematically represented at material level by using a spring model and a dash-pot model. This will, however, require a lot of springs.

1.4 *Outline of the investigation*

In this research, first a model has been set up for the description of the inertia and the

deformation modes, which have to be taken into account for a beam under transient loading conditions. As relatively very short wave phenomena may occur in the beam, it has been decided to implement in the model the theory according to Timoshenko. This means that translation and rotation inertiás well as bending and shear deformation are taken into account.
Next the solution method of the TILLY computer program has been evaluated and adapted for this research.
For the beam model used in this study, the required density of the geometrical discretisation has been determined, to be able to give a sufficiently accurate description of the high eigenmodes due to certain loading conditions. When the required number of elements had been determined, the maximum possible magnitude of the computing time step was analyzed, in order to get a reliable computation of the eigenperiods of the highest significant eigenmodes. An important property of this solution method is that with correct computation of the eigenperiod of a certain vibration, the amplitude will definitely meet the requirements of accuracy.
In the next phase the linear-elastic behaviour of the cross-section was extensively examined, to see to what extent the discretisation of the beam leads to deviations from the analytically known solutions for the response.
When the reliability of the models and the solution method had been sufficiently founded, some attention was paid to the way in which more complicated non-linear elastic behaviour of a concrete cross-section under bending conditions should be built into the model.
The response of elasto-plastic behaviour of the cross-section of a simply supported beam under a uniformly distributed explosion load (VEG) was determined and assessed. Different percentages of the maximum occurring bending moment under linear-elastic behaviour were used for the magnitude of the plastic moment. Later, the pure elasto-plastic behaviour of the cross-section was extended with hardening and its influence on the response has been studied.
In the last phase of the research two experiments were simulated. The aim was to establish to what extent the model used can be considered as a reliable means to predict damages that occur in physical reality. In this respect the maximum occurring (plastic) curvature and the permanent curvature after the tests are very interesting quantities. To improve the approximations, a new type of spring, the so-called "cycle-model" (Dutch: "wissel-model"), was added to the computer program.

2 Modelling

2.1 *Discrete schematic representation*

In Chapter 1 it was already mentioned that literature indicates that at least deformation due to bending and shear, as well as translatory inertia have to be included in a discrete model. This schematic representation corresponds with the Timoshenko theory, in which the rotatory inertia is rated zero. This schematic representation is sometimes called the bending-shear beam theory.

An important aspect that distinguishes the Timoshenko beam and the shear-bending beam from the simple Bernoulli-Euler beam, is the description of the propagation of the bending waves. In the Bernoulli-Euler beam the phenomenon occurs that the wave length and the propagation velocity of a bending wave are inversely proportional. This means that the physically possible maximum wave velocity is exceeded for short waves. The maximum velocity at which equilibrium perturbations may be transferred, equals the propagation velocity of longitudinal waves: $c_L = \sqrt{E/\varrho}$. Short to very short bending waves occur in a beam under an explosion load, especially when the load is highly impulsive. These waves propagate from the support or, in case of concentrated loads, from the boundaries of the load area to other parts of the beam. So, for the problems studied here, it is not sufficient to merely take into account bending deformation and translation inertia.

To obtain an upper limit to the propagation velocity of the bending waves, Rayleigh proposed to not only take into account the bending deformation and the translatory inertia, but also the rotatory inertia. As a result the upper limit of the propagation velocity of transverse waves becomes identical to the propagation velocity of longitudinal (dilatation) waves. This too is not physically realistic.

In very short bending waves the deformation due to shear becomes dominant (see Fig. 2). Therefore it is obvious that in the model, the deformation due to shear force has to be described well, which is the case in the Timoshenko theory. Also when the rotatory inertia is left out of the Timoshenko theory, resulting in the shear-bending beam, the upper limit remains correct. Fig. 2 shows that the cross-sections of the beam hardly rotate under short bending waves.

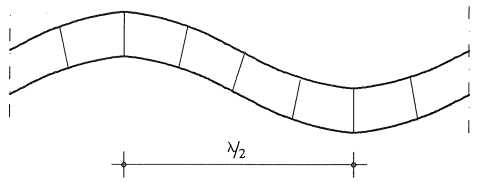

Fig. 2. The beam under a short bending wave.

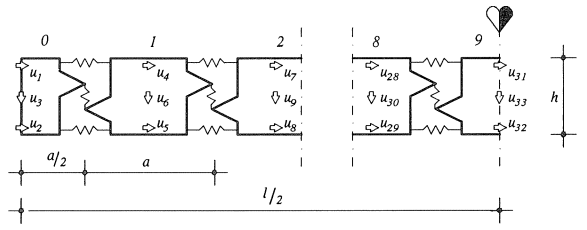

Fig. 3. Schematic representation of the beam.

The most logical conclusion seems to be that the discrete beam model has to contain bending an shear deformation as well as translatory inertia. It was, however, decided to also include rotatory inertia in the model, with which the model becomes a discrete

Timoshenko beam. This has been carried out by schematically representing the beam as a range of rigid elements, with three degrees-of-freedom each, connected to each other with springs, namely one spring for the shear and two springs that together allow the bending deformation.
In this research, the application of two springs for the description of the bending deformation was motivated by the phenomenon that concrete beams tend to elongate under bending conditions. This phenomenon is also called dilatancy. Whether dilatancy has a relevant influence on the results of the computations was not known when the model was set up. Therefore, the possibility to separately model the behaviour of the upper and the lower part has been built in. This also brings the possibility to simulate longitudinal processes with the model. This extra possibility has not been used in this research, however.
In the schematic representation of Van der Veen [9] no springs for shear are applied. Moreover, he takes few elements into account: 4 per half a beam length. For static loading conditions this is usually sufficient to clearly monitor the bending of the beam and especially the behaviour of the moments and the shear forces. In dynamic response, mainly the shear forces, but also the moments vary much more along the beam, so that a substantial increase of the number of elements per unit length is required.
In this research half a beam length contains at least 10 elements. Considering the arguments of symmetry, it is sufficient to discuss half the beam. With 10 elements the system then has 33 degrees-of-freedom, a number of which are fixed by the support conditions and the symmetry restrictions.
As has been mentioned in chapter 1, the program TILLY was used to the response of the model to explosion and collision loads. The user of this program has to specify the constitutive equation and the kinematic relation of the springs. The kinematic relation relates the deformation e of a spring to the degrees-of-freedom u. The relations between the degrees-of-freedom and the elongation of the spring can be determined with Fig. 4.

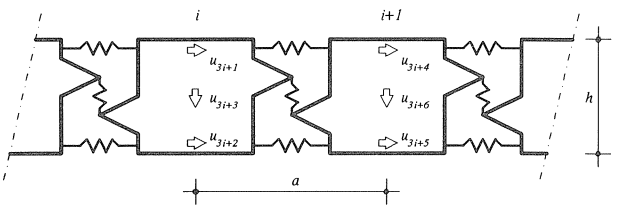

Fig. 4. Figure from which the relation between the degree-of-freedom u and the elongations e of the spring can be determined.

When, for purposes of readability, the element number i in Fig. 4 is set to 0, the elongation of the springs can be computed from the degrees-of-freedom u as:

$$e_1 = -u_1 + u_4, \tag{1}$$

$$e_2 = -u_2 + u_5, \tag{2}$$

$$e_3 = \frac{a}{2h}(-u_1 + u_2 - u_4 + u_5) - u_3 + u_6. \tag{3}$$

a being the element length and h being the effective height, that is to say the arm of the two forces that together constitute the bending moment.
The spring constants k are determined using the constitutive relations for the shear-bending beam:

$$M = EI\varkappa, \tag{4}$$

$$Q = \eta GA\gamma, \tag{5}$$

with

M = bending moment
E = Young's modulus of the material
I = stress moment of inertia of the cross-section
$\varkappa$ = curvature of the beam at the cross-section
Q = shear force
η = correction factor for the shear-stress distribution
G = shear modulus of the material: $G = E/2(1 + \nu)$
A = cross-sectional area
γ = the shear deformation of the beam at the cross-section

The bending moment M can be expressed in the spring forces $k \cdot e$ as (in the elastic domain and with normal force $N = 0$):

$$M = hk_2e_2 = -hk_1e_1 \tag{6}$$

The curvature $\varkappa$ can be written as:

$$\varkappa = \frac{e_2 - e_1}{ah} \tag{7}$$

In this study the upper and the lower springs are equal: $k_1 = k_2$. The result is that: $e_2 = -e_1$. Hence the curvature can be written as:

$$\varkappa = \frac{2e_2}{ah^2} = \frac{-2e_1}{ah^2} \tag{8}$$

Substitution of the curvature, expressed by the spring constants and the elongation of the springs, and the moment in the constitutive equations, results in the following spring constants for the upper and the lower springs:

$$k_1 = k_2 = \frac{2EI}{ah^2} \tag{9}$$

The same can be applied to the determination of the spring constant of the shear spring. Shear force Q can be written as:

$$Q = k_3e_3 \tag{10}$$

To the shear deformation γ applies:

$$\gamma = \frac{e_3}{a} \tag{11}$$

Substitution of both relations in the constitutive equations between the shear force and the shear deformation results in:

$$k_3 = \frac{\eta GA}{a} \tag{12}$$

To a rectangular cross-section of the beam applies:

$$I = \frac{bh^3}{12}, \tag{13}$$

$$A = bh, \tag{14}$$

b being the width of the cross-section and h being the overall height. Furthermore, assumptions were made for material properties of concrete concerning the lateral contraction (Poisson's ratio ν):

$$\nu = 0.2, \tag{15}$$

which, according to Mindlin [7] results in:

$$\eta = 0.8215. \tag{16}$$

The relation between the shear modulus and Young's modulus is:

$$G = \frac{E}{2.4}. \tag{17}$$

The assignment of values to the other quantities will be discussed later.
The translatory inertia m per element is:

$$m = \varrho A a, \tag{18}$$

with A = overall height × width. For the rotation inertia J applies:

$$J = \varrho b \int_{-h/2}^{+h/2} \int_{-a/2}^{+a/2} (x^2 + y^2)\, \mathrm{d}x\, \mathrm{d}z = \varrho I a \left(1 + \frac{a^2}{h^2}\right). \tag{19}$$

So not only the "axial rotatory inertia" but also the "lateral rotatory inertia" is taken into account.
The great advantage of this discrete schematic representation is that the still linear-elastic model can be relatively easily extended with, for example, non-linear springs and dash-pots. By varying the stiffness of the springs at the top and at the bottom of the beam, the beam dilatancy due to bending can also be described. The influence of shear deformation can easily be determined by varying the stiffness of the vertical springs. Cracking can also be simulated by linking springs in parallel. Besides, other loads than those considered here can be taken into account.

2.2 *Normalization of the model quantities*

It is possible to normalize the computations in such a way that the results for the deflection w, the moment M and the shear force Q are non-dimensional coefficients, which can subsequently be converted into a dimensional form by multiplication with dimensional quantities. This otherwise arbitrary choice was made as follows:

$$w = \bar{w} \cdot fl^4/EI \quad \text{c.q.} \quad w = \bar{w} \cdot Fl^3/EI \tag{20}$$

$$M = \bar{M} \cdot fl^2 \quad \text{c.q.} \quad M = \bar{M} \cdot Fl \tag{21}$$

$$Q = \bar{Q} \cdot fl \quad \text{c.q.} \quad Q = \bar{Q} \cdot F \tag{22}$$

with

l = length of the beam
f = distributed load on the beam
F = concentrated load on the beam

To make the formulas and quantities mentioned in the previous paragraph non-dimensional, the following expressions have to be introduced:

$$fl = 1 \quad (\text{c.q. } F = 1); \quad l = 1; \quad EI = 1 \tag{23}$$

The length-height ratio l/h and the Poisson's ratio ν, together with the dependent correction factor η for the shear stress distribution, are dimensionless. Chosen were $l/h = 20$ and $\nu = 0.2$ with $\eta = 0.8215$. In order to make an easy comparison with the work of Leussink [5], the value of l/h was chosen equal to 20. Usually beams have a smaller length-height ratio, often in an order of magnitude of 10. Plates generally have an order of magnitude of 20. For the spring constants the result is:

$$k_1 = k_2 = 2EI/(ah^2) = 16000 \tag{24}$$

$$k_3 = \eta GA/a = 32860 \tag{25}$$

Making non-dimensional with respect to time is usually done by rating the fundamental period of the beam equal to 1. This results in a certain value for the mass of the beam. Using this value in the computations, results in the time being expressed by the period time of the first eigenmode of the beam. Initially, the fundamental period of the simply supported Bernoulli-Euler beam has been used for the time unit. This was done similarly in the computations for the clamped beam.
The fundamental period of the simply supported Bernoulli-Euler beam is described by the following formula:

$$T^2 = \frac{4l^2}{\pi^2} \cdot \frac{\varrho A}{EI} \tag{26}$$

From this the translation inertia per unit length of the beam can be derived:

$$\varrho A = \frac{\pi^2}{4l^4} \cdot EI \cdot T^2 \tag{27}$$

For the mass belonging to the vertical (transversal) degrees-of-freedom, the choice of $T = 1$ and $a = h = l/20$ (10 elements on half the beam length) results in:

$$m_v = \varrho A a = \frac{\pi^2 T^2}{4l^4} \cdot EI \cdot \frac{l}{20} = \frac{\pi^2}{80} \tag{28}$$

For ϱIa can be derived:

$$\varrho Ia = \varrho A r^2 a = \frac{\pi^2}{384000}; \quad \left(r^2 = \frac{h^2}{12}\right), \tag{29}$$

which for J results in:

$$J = \varrho Ia \left(1 + \frac{a^2}{h^2}\right) = 2\varrho Ia = \frac{\pi^2}{192000} \tag{30}$$

The masses belonging to the horizontal (longitudinal) degrees-of-freedom can be derived from J as follows:

$$J = 2(h/2)^2 \cdot m_h \tag{31}$$

This results in:

$$m_h = 2J/h^2 = \frac{\pi^2}{240} \tag{32}$$

2.3 *Dimensionless wave velocities*

In order to interpret the response computed with the model more efficiently and to make a better founded choice for the computing time steps, it is useful to determine the values of three regularly used wave velocities from the quantities of the model, which have been derived in the previous paragraph. These velocities are:

the longitudinal wave velocity: $c_b = \sqrt{E/\varrho}$ (33)

the transverse wave velocity: $c_s = \sqrt{G/\varrho}$ (34)

the Rayleigh surface wave velocity: $c_R = c_s \cdot \sqrt{\eta}$ (35)

Substitution of the values derived for EI, GA, a, η, ϱAa and ϱIa results in:

$$c_b = \sqrt{\frac{19200}{\pi^2}} = 44.1[l/T] \tag{36}$$

$$c_s = \sqrt{\frac{8000}{\pi^2}} = 28.5[l/T] \tag{37}$$

$$c_R = c_s \cdot \sqrt{0.8215} = 25.8[l/T] \tag{38}$$

These velocities are very important for the choice of the computing time steps and for the interpretation of the results. It is, for example, a fact that transverse perturbation

cannot propagate through the beam with a velocity higher than the Rayleigh surface wave velocity. The longitudinal wave velocity is the upper limit of longitudinal perturbation. These phenomena have to be well described by the model.

3 A computer program for response computation

3.1 *The TILLY program*

To determine the response of the model set up in the previous paragraph, a special computer program for discrete elements was used. This program, called TILLY, contains, among others, a spring element and a dash-pot element.
Three types of material properties can be described with the spring element: linear-elastic, elasto-plastic with infinite deformation and elasto-plastic with finite deformation. The research described here starts with the linear-elastic problem, for which the spring element is definitely sufficient. After studying the linear-elastic domain, the attention is turned to the physical non-linear behaviour of a concrete beam. By linking a number of elasto-plastic springs in parallel, as available in TILLY, hardening in the non-linear behaviour of a concrete beam can be simulated.
The dash-pot element within the version of the TILLY program used, describes viscous damping. Just like the spring element, the dash-pot element can be connected with an arbitrary number of degrees-of-freedom by arbitrary kinematic constants.
Actually the equations of motion

$$\boldsymbol{K}v + \boldsymbol{C}\dot{v} + \boldsymbol{M}\ddot{v} = \boldsymbol{k}(t) \tag{39}$$

are formulated in TILLY. Broadly speaking, there are two basic methods to solve such a system. These methods are called "modal analysis" and "direct integration".
The first method converts the equation

$$\boldsymbol{K}v + \boldsymbol{M}\ddot{v} = \boldsymbol{k}(t) \tag{40}$$

to an eigenvalue problem. After solving the problem, the eigenvalues represent the resonance frequencies or eigenfrequencies, and the eigenvectors represent the vibration modes belonging to those eigenfrequencies. The load is expanded into a Fourier series and the solution is found by adding up a number of eigenmodes.
As this method is based on the principle of superposition, this method can only be used with linear problems, and therefore was not suitable as a method for the TILLY program.
The second method is directly developed from the equation of motion in (39). Assuming the starting conditions to be known, every integration takes place over a small time step. The resulting situation becomes the basis for the next time step, etc. A large number of methods are based on this principle. Examples are the central differential method, the Wilson θ method and the Newmark β method.
An integration method using a variational expression was chosen for the TILLY program. The method has been developed by A. W. M. Kok and is known as the Kok

γ method. The method is explained in [24] and [25]. A parameter γ occurs, which is used to control numerical stability. The value of γ^2 is chosen, depending on the case to be studied and the stability demands needed.

3.2 *Element density and time step magnitude*

Two important choices that have to be made in a discretised computation, are those regarding the element mesh and the time step, used in the process of the numerical solution.
The element mesh has to be chosen in such a way that local phenomena can be described as correctly as possible. This is closely related to the highest significant eigenmodes, which occur within a certain phenomenon. The highest eigenmode which can be correctly simulated by the model, has to be at least higher than the previously mentioned eigenmodes in the frequency domain.
The maximum time step can be determined when the highest eigenmode that has to be computed with sufficient accuracy, and the time step required by the computer program to be able to monitor an eigenperiod, have been established.
An extensive number of computations have been made with TILLY, in which attention was particularly focused on the accuracy of the shear forces. From this the following recommendations resulted.

Element mesh
In order to determine the required number of elements in the model, it is necessary to understand which eigenmodes still play a significant role in the response of the quantities deflection, bending moment and shear force. Conclusions concerning the element density may be drawn when this understanding leads to the establishment of the highest eigenmode, which the model must be able to describe. The shortest wave, which the model must be able to describe, can also be taken into consideration. In that case it has to be kept in mind that the shear force waves are normative, especially with the shortest loading periods used in this study.
It is a rule of thumb that the model can correctly describe a complete period with about 6 elements per wave length.

Time step
The importance of the accuracy of the periods of the highest eigenmodes of the model needs to be understood, in order to determine the time step with which the TILLY program can solve the model set up in this way. When the response shows phenomena, which, by their strong local character, indicate that they almost solely consist of the highest eigenmodes, it is very important that no phase shift between the highest eigenmodes occurs. A high and sharp peak in the time behaviour of a quantity consists of a coinciding group of high eigenmodes. In that case a phase shift may prevent the development of such a peak. This means that especially the time periods of these eigenmodes have to be computed very accurately, which requires a small computation time step.

Also the integration parameter γ^2 has to be rated at 2.
In these cases ($\tau_d < 0.1$), but also in cases in which the higher eigenmodes are less important, it is a rule of thumb that the computation time step should be about 1/5 of the period of the highest significant eigenmode.
In those cases where $\tau_d > 0.1$, $\gamma^2 = 0$ can be used for guaranteed numerical stability. When only the bending behaviour and the bending moment are of interest, the chosen time step may be larger. Usually, however, it would be preferred to compute the shear forces as correctly as possible.

4 Results of the investigations (linear-elastic)

This chapter reports on the computations with the TILLY program in the linear-elastic domain and their results. This study shows how the results under highly impulsive loading conditions (very short phase length, related to the fundamental period), may differ from the approach resulting from a computation in which the beam is modelled as a single mass-spring system. This is useful information for the designer.
The cases studied were subdivided into two main groups, namely the uniformly distributed load and the concentrated load. The uniformly distributed load is a load with a constant value per unit length, and covers the entire beam length. The concentrated load also has a constant value per unit length, but it does not cover the entire length of the beam, but only a part with a length equal to 1/20 of the beam length, situated in the middle of the span of the beam. The values for both types of load were taken in such a way that the overall load is the same for both.
The two time functions with five values for the characteristic rate parameter τ_d, the relative positive phase length, were studied for these two types of load distribution. The time functions are those of the explosion load (triangular load) and the collision load (symmetrical triangular load). The values of the relative positive phase length are: 10, 1, 0.5, 0.1 and 0.01. The way in which the beam was supported was also varied, namely simply supported and clamped.
All values of time are expressed in the fundamental period of the Bernoulli-Euler beam, taking into account the support conditions. Consequently the time span of the clamped beam is shorter than that of the simply supported beam. After all, the fundamental period of the clamped beam, is about 44 percent of the fundamental period of the simply supported beam [11].

4.1 *Uniformly distributed load*

The computations for a uniformly distributed load are carried out for all combinations of the parameters mentioned in chapter 1. The beam will either be simply supported or clamped (indicated by V and I respectively), for the load both the explosion load and the collision load will be considered (E and B) and all loading rates will be computed (1 to 5 inclusive).
Hereafter, the results are mainly presented in the form of tables. For one of the cases,

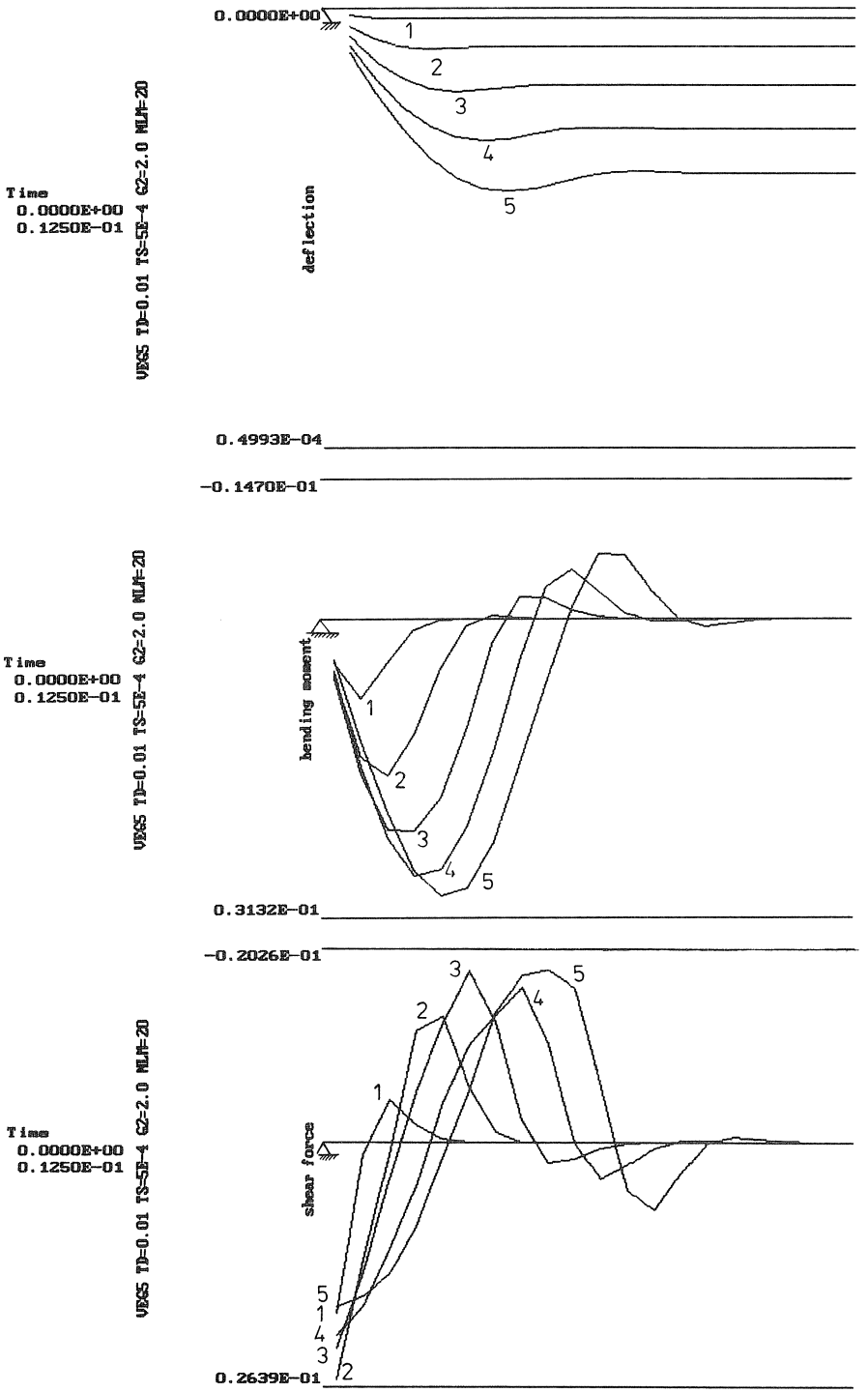

Fig. 5. The distribution of the deflection, the bending moment and the shear force along the beam at various points in time, for the case VEG5.

VEG5, some results are displayed graphically, so that the reader can gain an impression of the complexity of the problem and of the extent to which the response differs from the response that could have been expected when only the fundamental eigenmode would have been of interest (in fact a single degree-of-freedom system). In Fig. 5 the distribution along the beam of the deflections, the bending moments and the shear forces at a number of points in time, are given for VEG5.

4.1.1 DLF determination with the single mass-spring system

Based on the operative load distribution with time, the Dynamic Load Factor (DLF) can be determined with a single mass-spring system. This factor serves as a multiplication factor to establish the dynamic deflection and the dynamic bending moment, based on the static deflection shape and the moment line. This DLF cannot be used straightforwardly for the shear force at the support, since the elasticity in the single mass-spring system is directly related to the deflection in the middle of the field and not to the support reactions c.q. shear force at the support.
To determine the DLF for the support reaction the entire structure has to be considered. In setting up the single mass-spring system it was assumed that the bending line is constantly identical to the static deflection line under uniformly distributed loading conditions. Only the magnitude changes with time. This means that also the distribution of the velocity and the acceleration along the beam are identical to the static deflection line. The magnitudes of these quantities, however, are not in phase with that of the dynamic deflection line. With a free vibration the phase shift between the deflection and the velocity is 90 degrees. This also applies to the phase difference between the velocity and the acceleration. When the deflections reach their maximum positive value, the accelerations take their maximum negative value. Actually it always applies that the acceleration and the deflection take opposite directions and vary proportionally with each other.
Fig. 6 shows which forces and loads are acting on half the beam. The dynamic support reaction is denoted by $R(t)$, the distributed load by $f(t)$, the "inertial load" by $i(t)$ and the bending moment in the middle of the span by $\frac{1}{8} f_w(t) l^2$. The load f_w in the bending moment can be considered as "resistance" against the external, distributed load. The ratio of this force with the peak value of the load $\hat{f}$ equals the DLF(t). In the lower part of the figure the resultants of the distributed external load and the inertial load are denoted by $F(t)$ and $I(t)$. These resultants act at distances $l/4$ and $61l/192$ of the support respectively.

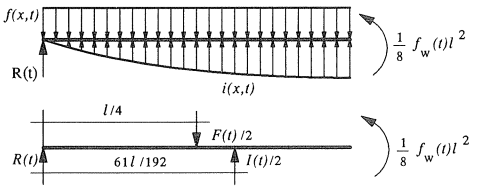

Fig. 6. Equilibrium of half the beam under inertial loading conditions.

From the equilibrium of moments around the point on which the inertial force imposes, follows:

$$\frac{61R(t)}{192}\,l - \frac{13f(t)l}{384}\,l - \frac{f_w(t)l^2}{8} = 0 \tag{41}$$

which can be elaborated into:

$$R(t) = 0.107f(t)l + 0.393f_w(t)l \tag{42}$$

Under static loading conditions the uniformly distributed load $\hat{f}$ results into a shear force equal to $\frac{1}{2}\hat{f}l$. To the DLF for the support reaction (and also the shear force at the support), therefore applies:

$$\mathrm{DLF}_R(t) = \frac{R(t)}{\frac{1}{2}\hat{f}l} = 0.214\,\frac{f(t)}{\hat{f}} + 0.786\,\frac{f_w(t)}{\hat{f}} \tag{43}$$

After substituting the expressions for $f(t)$ and f_w in the formula for the time function of the dynamic magnification factor of the support reaction (43), the maximum values of this factor can be determined. These values, as well as those for the deflections and the bending moments, are given in Table 3. The columns headed B refer to the collision load $f(t)$ (symmetrical triangular load) and the columns headed E refer to the explosion load $f(t)$ (triangular load). When $\tau_d = 0.01$, the maximum values of the DLF for the shear forces show a large dominance of the external load.

Table 3. Maximum DLF values of a single mass-spring system under a collision load (B) and an explosion load (E) according to Biggs [1].

		deflection		shear force	
τ_d	ωt_d	B	E	B	E
10	20π	1.00	1.95	1.00	1.74
1	2π	1.51	1.55	1.32	1.34
.5	π	1.27	1.20	1.01	.958
.1	$0.2\ \pi$	.312	.311	.245	.244
.01	0.02π	.0314	.0314	.214	.214

4.1.2 Maximum DLF values for distributed load

With a single mass-spring system, for a certain load one value of the DLF can be derived. This value applies to the deflection as well as the bending moments. The shear forces have another value. This is no longer valid in the case of an almost continuous beam. Then the DLF depends on the position at the beam and on the quantity discussed. The DLF for a quantity at a certain position is defined as the maximum occurring value of that quantity due to the dynamic load, divided by the value of that quantity at that position under a static load, which has the same magnitude as the dynamic load. When the momentaneous DLF for a quantity is plotted along the longitudinal axis of the beam, the result will be a graph, in which the deviation from the

horizontal distribution is a measure for the difference at the given point in time between the distribution of that quantity under static and under dynamic loading conditions. The same applies when the maximum value of the DLF is plotted along the beam axis. The resulting curve covers all momentaneous distributions. This line can be interpreted as a measure for the deviation of the strength of the design in relation to the statically loaded beam.

The cases VEG1 to VEG5 inclusive

In Table 4 the minimum and maximum values of the DLF are given as computed by TILLY, for the cases VEG1 to VEG5 inclusive. These are the values in the middle of the span for the moments and the deflections, and the values at the support for the shear forces. The values can be compared with Table 3.

Table 4. Minimum and maximum DLF values for deflection, moment and shear force, for the cases VEG1 to VEG5 inclusive (triangular load)

	deflection		moment		shear force	
τ_d	DLF_{max}	DLF_{min}	DLF_{max}	DLF_{min}	DLF_{max}	DLF_{min}
10	1.956	- .1083	2.016	- .1714	1.920	- .00263
1	1.556	-1.010	1.611	-1.066	1.463	- .8440
.5	1.194	-1.185	1.219	-1.221	1.153	-1.117
.1	.3069	- .3118	.3454	- .3496	.3996	- .3840
.01	.03149	- .03228	.04622	- .04618	.09194	- .08952

The agreement of the deflection is good for all values of τ_d, whereas the agreement of the moments can be called reasonable. However, the deviation of the shear forces is large for the smallest values of τ_d.

Now the maximum DLF value for the single mass-spring system is much larger than that of the discrete beam model, namely a factor of 2.3. It could, however, be stated that the assumption of the deflection shape being identical to the static one, is not at all valid for this type of loading. The determination of the dynamic support reaction with the single mass-spring system is strongly dominated by the external load and this is not confirmed by the response that was computed in a more refined way.

The cases IEG1 to IEG5 inclusive

The results of the computations of the maximum DLF values for the clamped beam under uniformly distributed loading conditions with varying τ_d, are given in Table 5. A characteristic difference with the previously computed response is that the clamped support causes an increase towards the middle of the beam, in the distribution along the beam of the maximum DLF for the bending moments. Apparently the clamped support causes the bending moment and shear force impulses applied to the beam, to be smaller than with the simple support.

Table 5. Minimum and maximum DLF values for deflection, moment and shear force, for the cases IEG1 to IEG5 inclusive, under triangular loading conditions.

	deflection		field moment		clamping moment		shear force	
τ_d	DLF_{max}	DLF_{min}	DLF_{max}	DLF_{min}	DLF_{max}	DLF_{min}	DLF_{max}	DLF_{min}
10	1.949	- .1005	2.045	- .09881	1.934	- .05488	1.840	0
1	1.553	-1.017	1.660	-1.075	1.530	- .9808	1.491	-.8954
.5	1.213	-1.198	1.383	-1.338	1.112	-1.120	1.057	-.9687
.1	.3026	- .3154	.4222	- .4447	.3632	- .3553	.4393	-.4443
.01	.03075	- .03175	.05742	- .06220	.04194	- .04582	.09354	-.09028

The cases VBG1 to VBG5 inclusive

The maximum and the minimum values of the DLF in relation to bending, moment and shear force, for the simply supported beam, under uniformly distributed loading conditions with a symmetrical triangular time behaviour, are given in Table 6. Compared with the series VEG1 to VEG5 inclusive, this series shows a number of characteristic differences. To begin with, the time function of the load for the case VBG1 contains such a slight slope that it might be called quasi-static ($\tau_d = 10$). Small dynamic effects only arise at the discontinuities in the time function. As the rising branch of the time function covers a period, which is equal to a whole number of fundamental eigenperiods of the beam, it is not surprising that the DLF_{max} is almost equal to 1.

Table 6. Minimum and maximum values of the DLF for deflection (w), moment (M), and shear force (D) for the cases VBG1 to VBG5 inclusive, under triangular loading conditions.

	deflection		moment		shear force	
τ_d	DLF_{max}	DLF_{min}	DLF_{max}	DLF_{min}	DLF_{max}	DLF_{min}
10	1.004	≈ 0	1.005	≈ 0	1.004	≈ 0
1	1.513	-1.283	1.540	-1.318	1.327	-1.085
.5	1.276	-1.275	1.312	-1.310	1.082	-1.080
.1	.3170	- .3173	.3709	- .3713	.3851	- .3842
.01	.03273	- .03257	.05198	- .04662	.09392	- .09208

When the relative positive phase length τ_d is equal to 1, the situation is already clearly dynamic.

For values of τ_d starting from 0.1 and smaller, the value of the DLF_{max} according to the single mass-spring system approaches $\pi\tau_d$. This can also be seen in the deflection when $\tau_d = 0.1$ and also within a 2 percent deviation, when $\tau_d = 0.01$. In the first case, the DLF_{max} deviates 18.5 percent for the bending moment in the middle of the span, and in the second case, the deviation is 66 percent. In both cases the shear force at the support deviates strongly. In the case $\tau_d = 0.1$, the TILLY calculation results in a 64 percent increase in the maximum DLF for the shear force. However, when $\tau_d = 0.01$, the model used in this study produces a maximum DLF value for the shear force, which is more than twice as small. This is a result of the fact that in the single mass-spring system the load has become dominant in the dynamic support reaction.

The cases IBG1 to IBG5 inclusive

The maximum and minimum values of the DLF regarding the deflection, the midspan moment, the clamping moment and the shear force of a clamped beam under uniformly distributed loading conditions, with a symmetrical triangular time behaviour, are given in Table 7.

Table 7. Minimum and maximum values of the DLF for deflection, moment and shear force for the cases IBG1 to IBG5 inclusive, under symmetrical triangular loading conditions.

	deflection		midspan moment		clamping moment		shear force	
τ_d	DLF_{max}	DLF_{min}	DLF_{max}	DLF_{min}	DLF_{max}	DLF_{min}	DLF_{max}	DLF_{min}
10	1.012	≈ 0	1.013	≈ 0	1.001	≈ 0	1.010	≈ 0
1	1.521	-1.303	1.581	-1.389	1.446	-1.196	1.276	-.9589
.5	1.283	-1.279	1.387	-1.372	1.186	-1.179	.9680	-.9545
.1	.3244	- .3305	.4333	- .4801	.3629	- .3686	.4168	-.4577
.01	.03076	- .03175	.05821	- .06252	.04201	- .04584	.09534	-.09153

4.1.3 Comparisons and conclusions

In paragraph 4.1.2, the results of the computations of the simply supported beam and the clamped beam under uniformly distributed loading conditions were discussed, using both the explosion and the collision load for the time function of the load.

It can be stated that the change of a collision load to an explosion load, the change of free support to fully clamped support and the change of larger values to smaller values of τ_d, cause the response of especially the higher eigenmodes to be more dominant. The overall response becomes "rougher". This can generally be seen in an increase of the DLF_{max} compared with that of the single mass-spring system.

Table 8 shows the deviations between the results of the single mass-spring system and those of the discretised beam model under uniformly distributed loading conditions. With these results, the region of application of both models can be determined, depending on the degree of inaccuracy that is acceptable.

When the acceptability is limited to 5 percent, the system with a single degree-of-freedom appears to be satisfactory for the deflections in all cases considered. For the bending moments in free supported beams the simple model is still satisfactory when $\tau_d = 0.5$ but not when $\tau_d = 0.1$. For clamped beams with the value $\tau_d = 10$ the limit of the applicability of the single mass-spring system with regard to the midspan moment has already been reached. For the determination of the clamping moment the simple model can be used as long as $\tau_d \geq 1$. Another rule of thumb can be derived for the shear forces. Now the form of the time function of the load appears to be a distinguishing factor (when $\tau_d \geq 1.0$). For these load durations the single mass-spring system can be used for the symmetrical triangular load but not for the step triangular load. When $\tau_d \leq 0.5$ the deviations for the triangular load are still the largest, but for neither form of loading can the single mass-spring system be used anymore.

Table 8. Differences in the results of the response computations using the beam model with multi-degrees-of-freedom and the single mass-spring system, related to the results of the model with multi-degree-of-freedom, expressed as a percentage

$$\left(\frac{1\text{mvs} - \text{nmvs}}{\text{nmvs}} \times 100\right).$$

For each combination the percentages of deflection, midspan moment and shear force are given one below the other. Where this is applicable, the clamping moment is given in brackets.

		uniformly distributed load				
		simply supported		clamped		
τ_d		collision (VBG)	explosion (VEG)	collision (IBG)	explosion-magnitude of (IEG)	order of all cases
10	w	0%	0%	- 1%	0%	0%
	M	0%	- 3%	- 1% (-1%)	- 5% (1%)	- 5%
	Q	0%	- 9%	1%	- 5%	- 10%
1	w	0%	0%	- 1%	0%	0%
	M	- 2%	- 4%	- 4% (4%)	- 7% (1%)	- 5%
	Q	- 1%	- 8%	0%	- 10%	- 10%
.5	w	0%	0%	- 1%	- 1%	0%
	M	- 3%	- 2%	- 8% (7%)	- 13% (8%)	- 15%
	Q	- 7%	- 15%	4%	- 7%	- 15%
.1	w	- 2%	1%	- 4%	3%	0%
	M	- 16%	- 10%	- 28% (-14%)	- 26% (-14%)	- 30%
	Q	- 36%	- 39%	- 41%	- 44%	- 45%
.01	w	- 4%	0%	2%	2%	- 5%
	M	- 40%	- 32%	- 46% (-25%)	- 45% (-25%)	- 45%
	Q	128%	133%	124%	129%	130%

Another interesting phenomenon, belonging to the "rougher" response to transient loads, is the fact that the shear force manifests itself more towards the middle of the beam. Especially with the shortest periods of loading, the maxima of the shear force appear to be constantly distributed over a large part of the beam, with a reduction in the zone in the middle of the span and a large increase in the support zone (see Fig. 7). Designers will duly have to take this into account and, in the case of a concrete beam, should definitely not reinforce the beam based on the static distribution of the shear force.

4.2 *Concentrated load*

The concentrated load is applied to the middle of the beam, over a length equal to $l/20$. This length is equal to the beam height. This choice is based on the original division of half the beam length into 10 elements, so that the external load is applied on the half element in the middle of the span. When the element grid is refined to thirty elements per half the beam length, the load is applied on one and a half elements in the middle.

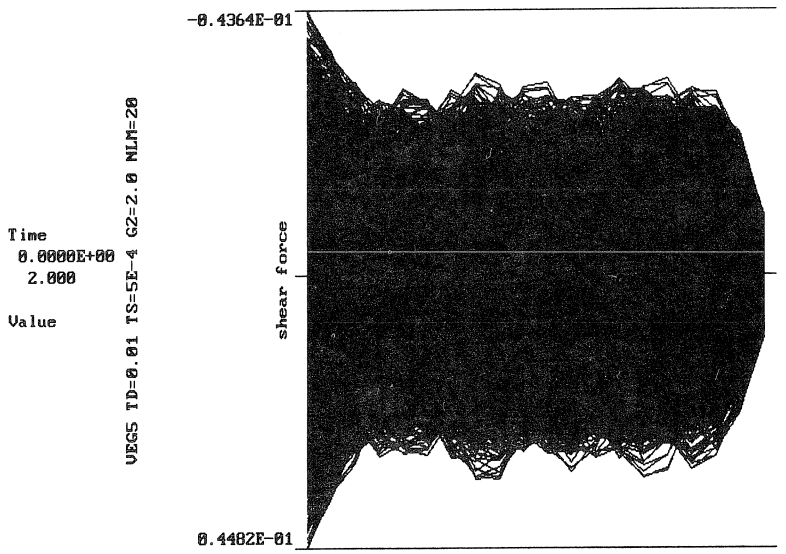

Fig. 7. The envelope of the shear forces in case of VEG5.

Fig. 8 shows the distribution of the deflections, the bending moments and the shear forces along the beam, at five computed points in time. The time interval between the lines is 0.0025 T. This is equal to ten times the computation time step. The successive lines are numbered 1 to 5 inclusive. It can be seen that the concentrated load causes bending waves and shear waves, which propagate from the middle of the span or, more accurately, from the edge of the load zone towards the support. The sharp peaks of the shear force at the edge of the load area are clearly visible. The fifth line shows that the shear force falls back when the load has disappeared. The deflection lines show that the movement in the middle of the span, at point in time 0.0125 T, is no longer an accelerated one. For, the increase of the displacement between 0.0075 T and 0.0100 T is larger than that between 0.0100 T and 0.0125 T.

Fig. 9 shows the plot with time of the shear force under loading VBP5, both at the edge of the load area and at the support. It shows clearly that the time function of the shear force, which is more or less sent as a signal from the edge of the load area into the beam, becomes visible at the support after a certain interval of time, be it with an opposite sign. The signal is reflected from the support and, after about the same interval of time as before, it can be recognized again from the variation of the shear force at the load area. As expected, a high peak value of the shear force occurs at the edge of the load zone. This value is more than 23 times as high as the value that would result from the application of the single mass-spring system.

Fig. 10 shows the distribution of the maximum values of the DLF for the bending moments. The static distribution of the moments with concentrated load is linear. Due to the impulsive character of the load in the case VBP5, the distribution of the moments becomes more constant over the length of the beam. So the support area of the beam is

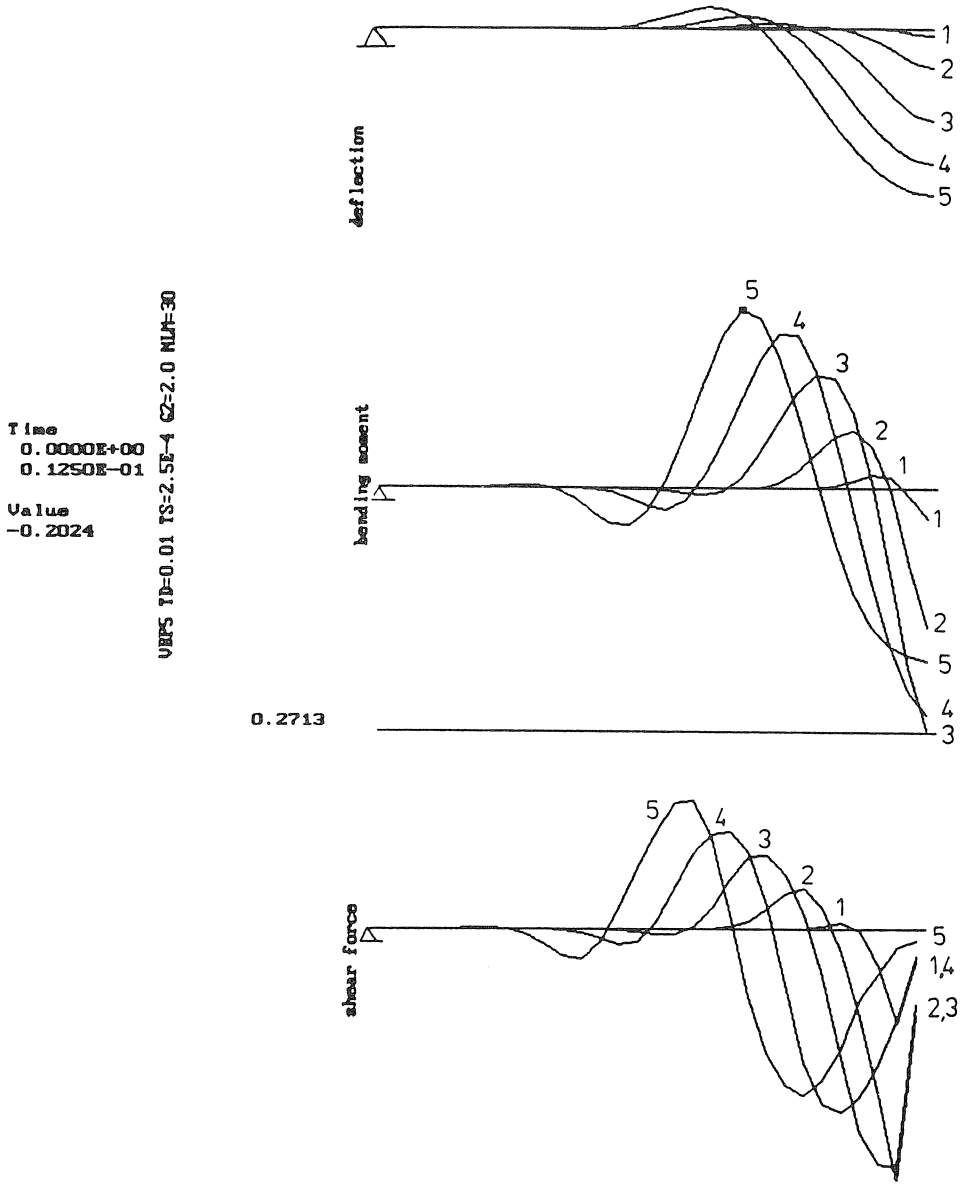

Fig. 8. The distribution of the deflection, the bending moment and the shear force along the beam for case VBP5 at various points in time.

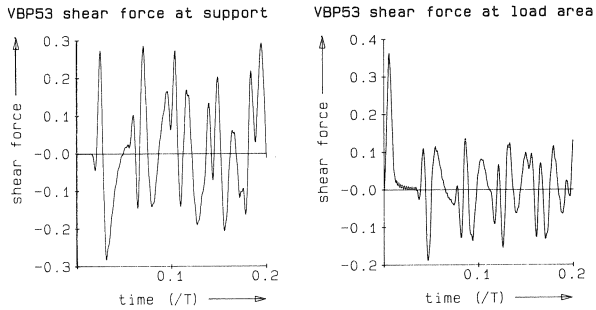

Fig. 9. The variation with time of the shear force for VBP5 at the edge of the load zone and at the support. The number of elements per half beam length is 30.

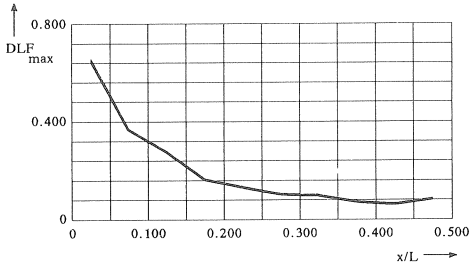

Fig. 10. The distribution along the beam of the DLF_{max} with regard to the bending moments of VBP5. The number of elements per half the beam length is 30. Only the points corresponding to those of the model with 10 elements per half the beam length have been drawn.

relatively heavily loaded for bending. The absolute maximum bending moment still occurs in the middle of the beam. So the edge of the load area is the normative cross-section in the case VBP5.

Table 9 gives the maximum values of the Dynamic Load Factor for the deflection and the bending moment in the middle, and the shear force at the support and at the edge of the load zone.

Table 9. Maximum values of the DLF for deflection, moment and shear force for the cases VBP1 to VBP5 inclusive.

	deflection (middle)	bending moment (middle)	shear force (support)	shear force (middle)
τ_d	DLF_{max}	DLF_{max}	DLF_{max}	DLF_{max}
10	1.004	1.003	1.012	1.000
1	1.495	1.360	1.790	.9984
.5	1.252	1.063	1.621	.9342
.1	.3230	.3839	.9742	.8810
.01	.03526	.09895	.5850	.7266

At this point it is also interesting to consider the results of the simple computations with a single mass-spring system. The forces acting on the beam have been drawn in Fig. 11. Because the shape of deflection is different from that of the uniformly loaded beam, the inertial force imposes at $\frac{8}{25}l$ of the support. In the half beam discussed, the external load is half the concentrated load and acts at the middle of the span.

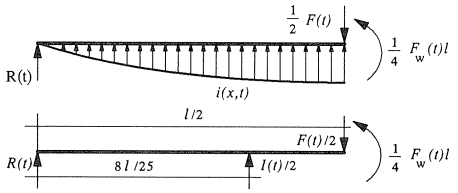

Fig. 11. Dynamic equilibrium of half the beam under concentrated external loading conditions.

The dynamic equilibrium equation can be formulated by considering the moments of equilibrium around the point of impact of the inertial force.
The equation is:

$$\frac{8}{25}R(t)l + \frac{9}{100}F(t)l - \frac{1}{4}F_w(t)l = 0 \tag{44}$$

in which $F(t)$ represents the concentrated load in the middle of the beam and $F_w(t)$ the apparent "resistance force" against the external load, which forms the bending moment in the middle. For the Dynamic Load Factor, regarding the shear force at the support, follows:

$$\mathrm{DLF}_R(t) = \frac{R(t)}{\frac{1}{2}\hat{F}} = -\frac{9}{16}\frac{F(t)}{\hat{F}} + \frac{25}{16}\frac{F_w(t)}{\hat{F}} \tag{45}$$

$\hat{F}$ being the peak value of the load function with time. This formula can be substituted in the solution for the response of the single mass-spring system, which was given in the previous paragraph. Table 10 shows the results for the five values of τ_d. In this table, values for $\tau_d = 0.1$ and $\tau_d = 0.01$ that initially are dominated by the load, are given in brackets. These values are negative because the concentrated load that imposes to the right of the resultant of the inertial force, dominates the bending moment.

Table 10. Maximum DLF with respect to the dynamic support reaction under concentrated loading conditions.

τ_d	$\mathrm{DLF}_{R,max}$
10	1.010
1	2.026
.5	1.989
.1	.4868 (-.5369)
.01	.04906 (-.5622)

The variation of the maximum DLF for the deflection is close to the results of the multi-degree-of-freedom model when $\tau_d \geq 0.5$. When τ_d is equal to 0.1 the deviation is 3% and when $\tau_d = 0.01$ it is already up to 11%. Both deviations concern underestimations by the single mass-spring system, which are clearly larger than with a uniformly distributed load. When $\tau_d = 10$, the bending moment in the middle corresponds well. When $\tau_d = 1$ the simple model renders an overestimation of 11%. When $\tau_d = 0.5$ this has already increased to 19%. When $\tau_d \leq 0.1$ this tendency reverses strongly. When $\tau_d = 0.1$ the single mass-spring system renders an underestimation of 19% and when $\tau_d = 0{,}01$ it even renders an underestimation of 97%.
The maximum DLF value for the bending moment appears to become of the same order of magnitude as that of the shear force at the support under uniform loading conditions. Perhaps this is a parallel. The DLF values of the shear forces with $\tau_d \leq 1$ deviate considerably from those of the single mass-spring system. Only the shear force at the support (dynamic support reaction) shows a tendency in the same direction, even though the deviation of the single mass-spring system with regard to the beam model is 13%.
The shear forces at the edge of the load zone are not represented in the simple single degree-of-freedom system. Therefore it is not surprising that the DLF_{max} for this quantity, computed with the TILLY model, can be compared with neither the DLF nor the DLF_R from the simple model.
For this reason it is concluded that the single mass-spring system may not be used for the shear forces in the vicinity of the load area.

5 Elasto-plastic modelling

5.1 *Choice of moment-curvature relation*

In the study concerning the linear-elastic model, the response has been determined for several combinations of the load distribution, the time function of the load and the type of support. Also the maximum occurring bending moment has been determined. Considering this moment, which occurs under linear-elastic behaviour of the cross-section, a designer may wonder whether this moment should really be carried fully linear-elastic. Practice holds the opinion that this is not necessary. By allowing plastic deformations in the structure, energy is dissipated and redistribution of moments in the structure will come about. This means that the designer may choose a plastic moment smaller than the maximum occurring bending moment with linear-elastic behaviour. The question is how far this reduction may be allowed to go. The smaller the yield force, the larger the plastic deformation will be.
In the previous chapters linear-elastic material behaviour has been assumed. Concrete was only involved in the application of the value 0.2 of the Poisson's ratio ν. All other quantities, such as the bending stiffness EI of the cross-section and the density ϱ were normalized.
Concrete, however, shows behaviour for which the linear-elastic theory is only valid to

a limited extent. A beam of reinforced concrete shows even more complicated behaviour. Aspects such as cracking of the concrete, plastic yielding and slip of the reinforcement, the influence of existing shear force on rotation capacity, tension-stiffening/softening, aggregate interlock etc. may be included in the description of this behaviour. There is no need to take all these aspects into account. To reach the objective of this study the use of a non-linear relation between the moment and the curvature will be sufficient. This can be described by a tri-linear diagram: one linear-elastic non-cracked branch, a branch for the cracked stage and a branch for the yielding of the reinforcement, see Fig. 12a.
The yielding of the reinforcement causes large plastic curvatures to arise, so that much energy can be dissipated. The vertical shading in Fig. 12a shows the contribution of tension-stiffening to this energy dissipation in the cross-section. With large plastic rotations this contribution is small in relation to the overall energy dissipation (both the vertical and the horizontal shading). This means that a bi-linear diagram will be a good approximation, even more so when the plastic curvatures become sufficiently large. In case of unloading the stiffness of the elastic branch is retained. This M-$\varkappa$ diagram is shown in Fig. 12b.

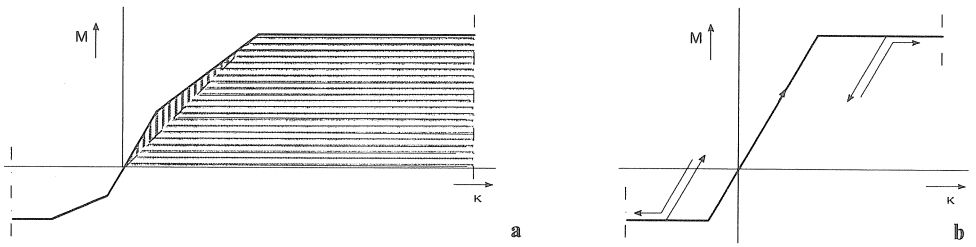

Fig. 12. Moment-curvature relation.
a. Tri-linear elasto-platic constitutive relation with crack.
b. Bi-linear elasto-plastic constitutive relation.

5.2 *Ductility*

In this study the occurring ductility μ of a spring is understood to be the quotient of the occurring plastic deformation of the spring during the computation and the maximum possible elastic deformation, or yield strain, of that spring, see Fig. 13. The occurring ductility is also called the ductility demand. This quantity plays an important role in assessing whether the rotation capacity of the structure is sufficient. It is pointed out that the definition of ductility differs from what many other people hold it to be. Ductility is often associated with the plastic deformation at collapse. In this study this ultimate ductility will be denoted by μ_u.
There is ductility demand at every point in a continuous structure. This may be either positive, zero or negative. In the beam model used in this study, ductility arises at every cross-section containing bending springs. The situation is somewhat more complicated in the case of cyclic yielding. Then we may speak of a ductility demand and an accumu-

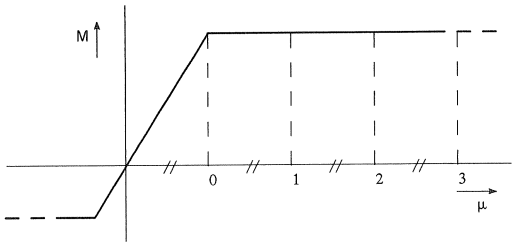

Fig. 13. Definition of ductility.

lated ductility demand. The ductility demand is directly related to the momentaneous occurring plastic deformation. So this is reduced again by a negative plastic deformation and might change its sign. In the accumulated ductility the absolute values of all plastic deformations of the spring are totalized. Therefore, it can only increase or remain the same. For reasons of assessment of the extent of damage of the construction the accumulated ductility demand is of interest. However, it is still not clear how this assessment should be made. The ductility demand is discussed in this study.

5.3 *Rotation capacity*

Plastic deformations in beams usually arise locally and manifest themselves as plastic hinges. In the schematic representation of a computation it is a point, but in reality the plastic curvatures occur over some length of the beam. This length is of the order of the beam height. Over this length the plastic curvature is not equal in size. The integral of these plastic curvatures is called the plastic rotation of the hinge. The largest allowable plastic rotation is called the rotation capacity of the structure. An important question is whether the rotation capacity is sufficient in structures under dynamic loading conditions that develop elasto-plastic deformation. In other words: is it larger than the maximum occurring plastic rotation under dynamic loading conditions.
Much is known about the rotation capacity of a cross-section of concrete under static loading conditions. When the distribution of the bending moment and the shear force along the beam is known, the size of the area that contributes to the plastic rotation can be determined, by using either more simple or more complicated models. When the length of the full plastic hinge is known, the relation between the plastic rotation and the plastic strain of reinforcement steel may be found. Under static loading conditions, hot rolled steel can often undergo a plastic strain in the order of 5 to 10% [13]. The concrete pressure zone often collapses under that strain. Under dynamic loading conditions the phenomenon occurs that the plastic zone shortens, resulting in a larger steel strain, with the same plastic rotation as under static loading conditions. This is because the extension is produced by a shorter length of the steel. The dynamic computation model will have to be able to correctly describe this shortening of the plastic zone.
On the other hand the question is, how exactly will the concrete pressure zone behave under the rapid deformation of the cross-section? In the rotating cross-section there is

an enormous gradient in the strain rate (compression) of the concrete. The ultimate concrete "fibre" will deform most rapidly, and in a first approximation the strain rate shows linear reduction towards the neutral line. Using the knowledge that concrete shows more softening when tested rapidly under pressure, may imply that the fibers with maximum stress are situated more towards the middle. This could have an enlarging effect on the rotation capacity.
In the much used handbook TM 5-1300 [12] it is recommended to take into account a maximum possible rotation of the plastic hinge of 12 degrees. However, this recommendation appears to be based on tests under static loading conditions. Experiments with plates under dynamic loading conditions [13], carried out by the "Prins Maurits Laboratory" of the TNO Institute, showed however, that the reinforcement already fractured with a rotation of 8 degrees. Tests under static loading conditions with the same series of test material, showed that the reinforcement did not even fracture with a rotation of 22 degrees.
It will be clear that criteria for collapse, concerning the fracture of the reinforcements, are hard to give. The tendency is clear, however, that the rotation capacity decreases under dynamic loading conditions.
Experiments [13] showed that the yield strength of the reinforcement increased by about 20%. Others detected an increase in the order of 10 to 15 %, with the strain velocities that occurred in the experiments [14], [15] and [16].
From various investigations it appeared that the rotation capacity depends on the simultaneously occurring shear force, see reference [9]. The larger the shear force, the smaller the rotation capacity. Views on the exact correlation of these two quantities differ.

5.4 *Objective of the elasto-plastic computations*

The elasto-plastic computations carried out, were meant to explore the most important differences that arise in elastic computations when a plastic limit for bending is applied. Not all elastic computations were repeated, but a selection was made.
Table 1 is referred to for the codes used to denote the combination of support, load time function and load distribution.
It was decided to only consider a simply supported beam (case V). The elastic moment lines suggest that the most spectacular changes will occur in this case. Furthermore only the uniform (G) explosion load (E) is discussed. The explosion load was preferred over the collision load because the explosion load keeps a dynamic character, independent of the extent of the positive phase length. This is caused by the jump in the time behaviour of this load. With increasing t_d, the collision load, as modelled in this study, becomes a more and more gently increasing branch and so becomes quasi static.
For the loaded beam chosen, two parameters are varied, namely:
- the magnitude of the full plastic moment;
- the loading rate (duration t_d or τ_d).

It is considered beyond the aim of this study to develop criteria for collapse. This study

is to supply information on occurring bending moments, shear forces and deformations. So, it informs on the demand for strength and deformability. These can be compared with knowledge from other sources about the acceptable quantities and/or combinations of quantities.

6 Results of the investigations (elasto-plastic)

In this chapter the plastic computations described in paragraph 5.4. are carried out. Paragraph 6.2 concerns the shortest load duration, which is examined in the elastic computation ($\tau_d = 0.01$) of the simply supported beam, under an explosion load. So it deals with an extension of the elastic case, which was denoted by VEG5 in the previous chapters. For this loading rate a number of values of the plastic moment will be examined.
In paragraph 6.3 the effect of a longer load duration ($\tau_d = 0.1$) will be examined, again for a number of values of the plastic moment. This applies to the case VEG4. Paragraph 6.1 will describe how the choice of the magnitude of the plastic moment is made.

6.1 *Quantification of the elasto-plastic model*

In the study regarding the linear-elastic model, the response of several combinations of support, load distribution and time function of the load has been determined. Also the maximum occurring bending moment has been established.
In this chapter the magnitude of the plastic moments is chosen to be a percentage of the maximum occurring bending moment with elastic behaviour. These percentages have been established at 50, 40, 30 and 20. The ductility demand for these four values is expected to increase respectively. Also the cross-sections of the beam closer to the support are expected to yield if the plastic moments are lower, because local maxima develop in the initial phase of the response, which may already exceed the plastic moment. The four elasto-plastic computations based on VEG5, will be denoted by the codes: VEG5P5, VEG5P4, VEG5P3 and VEG5P2. The letter P denotes plasticity and the final digit denotes the decade of the percentage of strength. The maximum bending moment in the elastic computation of VEG5 is 0.00577 ($\cdot fl^2$). The plastic moments of the four cases mentioned above are given in Table 11.

Table 11. Plastic moments of the computed elasto-plastic beams.

case	$M_p(\cdot 10^{-3} pl^2)$
VEG5P5	2.89
VEG5P4	2.31
VEG5P3	1.73
VEG5P2	1.15
VEG4P4	17.2
VEG4P3	12.9
VEG4P2	8.59

In the case of VEG4, the maximum value of the bending moment with linear-elastic properties of the cross-section is 0.0423 ($\cdot fl^2$). Due to limitations in time and space, the computation with the 50 percent plastic moment has not been carried out. However, for a comparison with the shorter phase length $\tau_d = 0.01$, this is no great problem. The three cases computed will be denoted by the codes VEG4P4, VEG4P3 and VEG4P2. Also these plastic moments are given in Table 11. Because of the occurrence of higher frequency phenomena, the model with 20 elements per half the beam length has been used in the elasto-plastic computations of VEG4.

6.2 *Results of VEG5P*

Time behaviour

The Figs. 14a and 14b show two illustrative results of the computation VEG5P of the variation with time of the bending moments in the middle of the span ($x = 0.4875l$) and of the shear forces at the support ($x = 0.0125l$). Fig. 14a shows the linear-elastic case and Fig. 14b shows the results of the elasto-plastic model. The scale on the vertical axes is kept constant for both figures (for the definition of R_{const} see page 49).
It is clearly visible that the sharp peaks, caused by high eigenmodes, strongly reduce in value with the variation of the bending moments with time. The fact that there is an upper limit to the bending moment naturally causes a limitation of the maximum value of the occurring bending moment, but it also shows that there are no more high and sharp peaks in the remaining vibrations after the end of the plastic phase has been reached (when the maximum deflection occurs). So the occurrence of plastic zones results in the higher eigenmodes attenuating out of the response.
Also the high peak values in the time plot of the shear forces are flattened as a result of the presence of plastic rotations.

Yielding areas

A clear insight into the development of regions in the beam where yielding occurs can be gained with the FILM program, which was developed for this study. With this program the output of TILLY can be visualised in such a way that deflection lines, moment lines and shear force lines are projected onto the screen, and are updated per time step. This method of projection is also called animation. In order to be able to record certain information for reports, the possibility to plot collections of lines belonging to several points in time, has been added to the program. Within the program this method of projection is called "cumulative mode".
The FILM program was also used to study the output of the linear-elastic case VEG5. Observing the results the following remarks can be made. At the support a perturbation develops in the form of bending and shear. This perturbation propagates as a wave phenomenon towards the middle of the span, showing an increase in the value of the bending moment. In the elasto-plastic case, the plastic moment will be exceeded at a certain point. If this point is situated between $0.0125l$ and $0.2125l$ (corresponding to the model) the plastic zone may shift towards the middle of the span. This phenomenon of

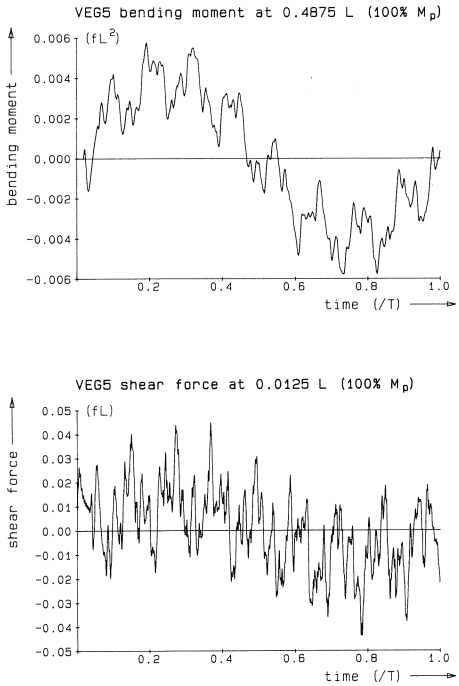

Fig. 14a.
Time plot of bending moments and shear forces in the linear-elastic case VEG5.

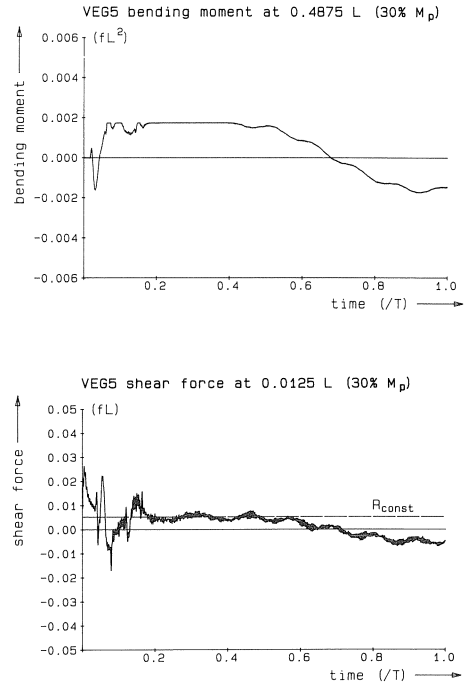

Fig. 14b.
Time plot of bending monents and shear forces in the elasto-plastic case VEG5P3 (plastic moment 30%).

the "shifting plastic hinge" has also been observed by Van der Veen [9]. Considering the eventual occurrence of maximum moments and deflections at the middle of the span, the plastic hinge is generally expected to shift towards the middle of the span.
In this study, however, it appeared that this expectation is based on too simple a conception of the physical reality, as if the perturbations would propagate only monotonous and only once towards the middle of the beam. In the beam used in this study, having a length-height ratio of 20, the bending wave propagates through the beam at such a velocity, that, at a given point in time, the wave from the other end of the beam exceeds the current moment distribution. This leads to a shift of the top in the moment distribution, towards the support, for a certain interval of time. This is shown in Fig. 15. The region in which this phenomenon occurs is situated between $0.1875l$ and $0.3125l$. So, in this region a "shifting plastic zone" may occur, which for some time shifts towards the support. This depends on the value of the plastic moment of the beam with respect to the height of the wave peaks in the linear-elastic case.
Diagrams can be made in which the beam length is given horizontally and the time vertically, to understand the occurrence of plastic deformations with time. The occurrence of yielding in a certain cross-section during a certain time step is denoted by a horizontal bar. The occurrence of yielding is understood to be an increase or decrease

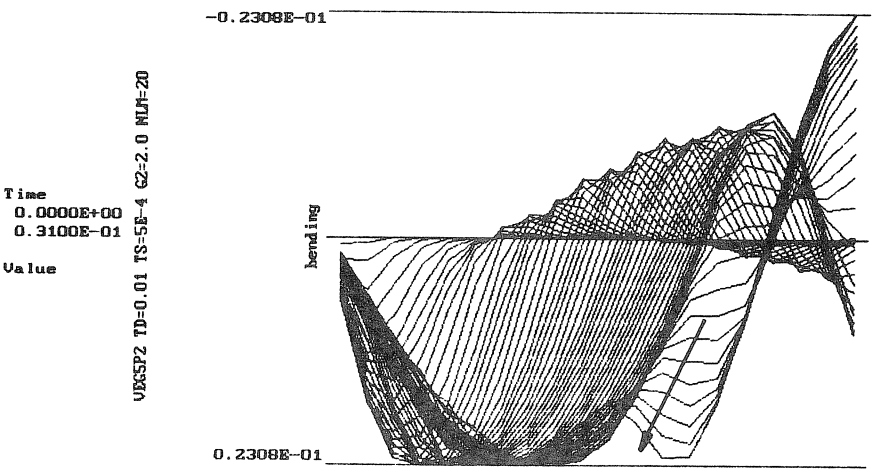

Fig. 15. Bending moment waves in the direction of the support.

of the plastic deformation in the time step concerned. The intervals of time in which yielding occurs appear as "black" regions in the diagrams. Fig. 16 shows the diagrams of the four plastic moments of the case VEG5P.
In the upper half of this figure, a smaller time scale was used than in the lower part, so that the shifting plastic zones in the initial phase are clearly visible. The lower figure shows how the plastic period is lengthened by lower plastic moments and concentrates at the middle of the beam.
The figure does not show the values of the plastic deformations. To also show the variation of the values of the ductility demand, colours or shades of grey could be used. In the next paragraph, graphs are shown, in which the ductility distribution along the beam is given. A combination of the figures 16 and 17 in the following paragraph leads to the conclusion that the length of the plastic period shows a large correlation with the magnitude of the occurring plastic deformations.

Ductility

Fig. 17 shows the ultimate ductility of each cross-section in the model, for the four computations. It is clear that a lower plastic moment results in a larger ductility demand. Each time, the dominance of the ductility demand in the middle cross-section is striking. In all cases, however, a local maximum also occurs at a certain distance from the middle. These maxima occur earlier in time and might be normative for collapse. In the case VEG5P2, the maximum ductility of 37.1 occurs at the middle of the beam. The acceptable ductility of the concrete cross-section was beyond the scope of this study. The question is whether a ductility of 37.1 is "very much". From remarks received it appeared that locally this value is definitely conceivable. Values of a "global" ductility at structural level are generally thought to be in the order of 5 to 10. This way of approach is similar to the way in which the structure is schematically represented by "global" quantities such as deflection at the middle, maximum bending moment, etc.

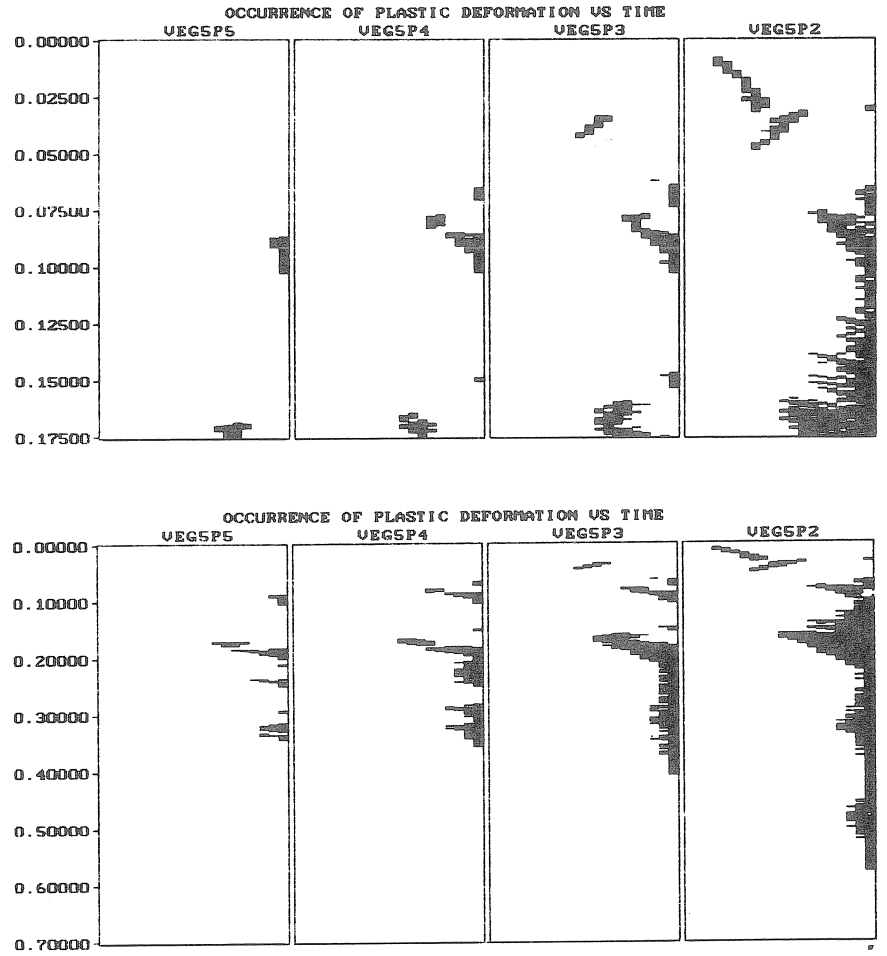

Fig. 16. The position of the plastic zones along the beam in time, for the cases VEG5P5 to VEG5P2 inclusive.

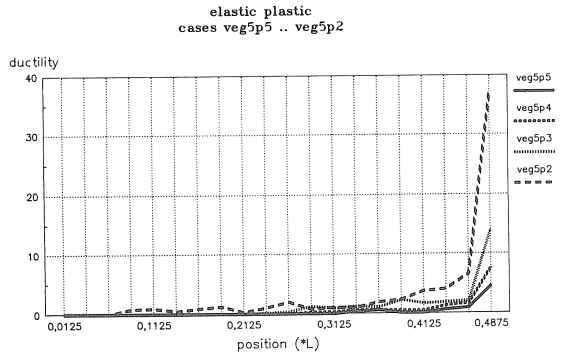

Fig. 17. Ultimate ductility distribution along the beam (VEG5P5 to VEG5P2 inclusive).

6.3 *Results of VEG4P*

In the previous paragraph the explosion load with a relative positive phase length of 0.01 was applied (VEG5). For the case in which the duration of the load is ten times as long (VEG4), three elasto-plastic computations were carried out. These concerned plastic moments of 40, 30 and 20 percent respectively. This paragraph elaborates on the yielding zones and the ductility demand.

Yielding zones

Fig. 18 shows the development of the yielding zones for the three plastic moments. In the upper half the initial phase is shown in detail. The lower half shows a time interval, which completely includes the plastic period of the case VEG4P2.

Compared with the three corresponding cases with $\tau_d = 0.01$, a plastic moment with a longer duration appears to occur in the middle cross-section. In the case VEG4P2 a transient, shifting plastic zone towards the support occurs. Compared with the cases VEG5P the duration of plastic deformation around the middle cross-section tends to be more dominant when the plastic moment decreases. A concentration effect of the plastic rotation towards the middle cross-section occurs with a longer relative positive phase length.

Ductility

Fig. 19 shows the distribution along the beam axis, of the ductility demands.

Here, a larger value as well as a larger concentration of the ductility occurs, compared with the calculations with $\tau_d = 0.01$. This could be expected: more impulse is applied to the beam, which results in a larger initial kinetic energy. This has to be converted into potential energy, elastic deformation and heat by means of plastic deformation. If the maximum elastic deformation energy was the same in the cases VEG5 and VEG4 this would be obvious, but here it is not. In the cases VEG4P4 to VEG4P2 inclusive, the plastic moments were assumed to be related to the maximum bending moment in the elastic case VEG4. This maximum elastic bending moment in the case VEG4 is: 0.04296 ($\cdot fl^2$) and in the case VEG5 it is 0.005770 ($\cdot fl^2$). So in the linear-elastic case VEG4, an impulse, which is ten times larger, results in the maximum bending moment increasing by a factor of 7.45. This means that an increase of the impulse by lengthening of τ_d, in the linear-elastic case, results in a moderate increase in magnitude of the bending moments. So the beam is related to the amount of kinetic energy applied, which in this research was weaker with $\tau_d = 0.1$ than with $\tau_d = 0.01$. To what extent this can be held fully or partly responsible for the increase of the plastic deformation with a longer τ_d has not been examined, but the conclusion that this is true seems to be justified.

6.4 *Interpretation with the single degree-of-freedom system*

In the two previous paragraphs it has become clear that a pronounced plastic hinge becomes visible in the middle of the span, resulting from a complex play of shifting

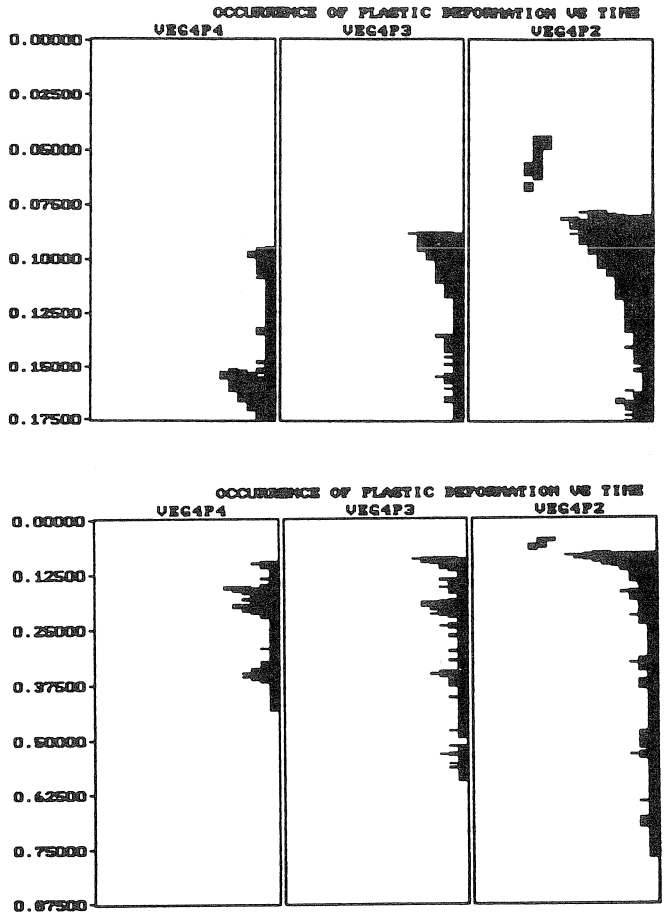

Fig. 18. The variation of the plastic zones along the beam with time, of the cases VEG4P4 to VEG4P2 inclusive ($\tau_d = 0.1$).

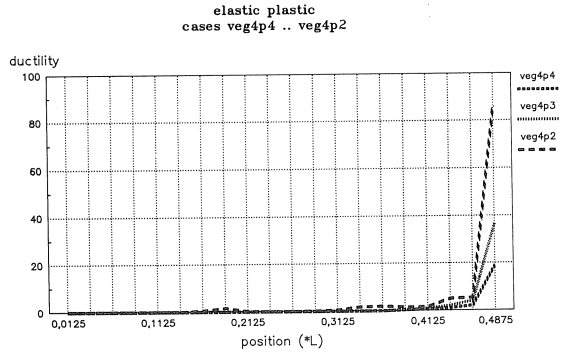

Fig. 19. Distribution of the ultimate ductility along the beam with $\tau_d = 0.1$ (VEG4P4 to VEG4P2 inclusive).

plastic hinges over large parts of the beam length. This can clearly be seen in all seven computations. This leads to the assumption that it should be possible to fairly accurately determine the maximum deflection and the plastic rotation with the single degree-of-freedom system as shown in Fig. 20. The quantities used in this model are also indicated in the figure.

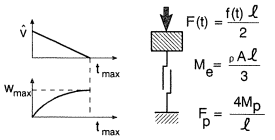

Fig. 20. The plastic single degree-of-freedom system.

In the schematic representation, the assumption was made that the only possible deformation consists of a plastic hinge at the middle of the field. The adjacent beam halves on either side, are assumed to be straight and it is assumed that the full plastic moment immediately occurs in the plastic hinge at time $t = 0$. Actually this kinematic model describes incremental deformation from the moment the plastic time interval is entered. The application of this model as a complete description of the beam behaviour implies a sudden change in the properties of the dynamic system. When, however, the plastic rotation in the middle of the span is sufficiently large, the resulting inaccuracy is negligible. The quantities shown in Fig. 20, concern equivalent quantities as far as the beam properties are concerned. The equivalent mass is determined by equating the kinetic energy for the single degree-of-freedom system and the beam:

$$0.5M_e\hat{v}^2 = \int_0^l 0.5\varrho A v^2(x)\,\mathrm{d}z$$

Taking into account the linear distribution of the velocity along the beam, it follows for the equivalent mass:

$$M_e = \frac{\varrho A l}{3} \tag{46}$$

The plastic resistance force F_p of the single degree-of-freedom system is found by equating the full plastic moment M_p to the moment resulting from a concentrated load F_p half way along the beam:

$$F_p = \frac{4M_p}{l} \tag{47}$$

Assuming that t_d is small compared with t_{max}, an impulse i is added per beam length unit in the order of magnitude:

$$i = \frac{1}{2}\hat{f}t_d,$$

in which $\hat{f}$ = the peak value of the load at $t = 0$.

Because of this the uniformly distributed mass ϱA gets a uniformly distributed velocity v_0:

$$v_0 = \frac{\hat{f} t_d}{2\varrho A}$$

This velocity distribution is obstructed at the support. Conversion of the uniformly distributed velocity into a linear velocity along the beam should be achieved by applying an impulse at the supports. The magnitude of this impulse should be such that the velocity of the beam becomes exactly zero at the support. Applying an impulse at the end of a previously motionless beam causes a translation velocity and a rotation velocity in the beam. The resulting centre of rotation of the movement of the beam is at $2l/3$ from the end where the impulse is applied. The vertical velocity at the side of the impulse is twice as large as at the other end. So a velocity input at the side of the impulse of magnitude $-v_0$ leads to a velocity increase of $v_0/2$ at the other end. This beam corresponds to the half beam from the model with a plastic hinge in the middle of the span. So, as a result of the impulse at the support, the velocity in the middle of the beam becomes equal to 1.5 times the original uniformly distributed velocity (see Fig. 21). The initial velocity $\hat{v}$ of the equivalent mass M_e is formulated as follows:

$$\hat{v} = \frac{3}{2} v_0 = \frac{3}{4} \frac{\hat{f} t_d}{\varrho A} \tag{48}$$

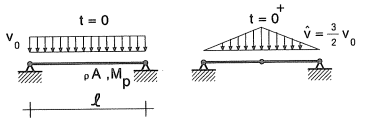

Fig. 21. The determination of the velocity distribution in the plastic case.

In the plastic phase the spring force on the mass is constant and takes the opposite direction of the velocity. Therefore, according to Newton's law, the velocity decreases linear with time. The point in time at which the velocity becomes zero, is the point in time t_{max} at which the maximum deflection is reached.
t_{max} is formulated as:

$$t_{max} = \frac{M_e \hat{v}}{F_p} + \frac{\hat{f} t_d l^2}{16 M_p} \tag{49}$$

The time interval from 0 to t_{max} can be regarded as the plastic time interval. This interval can also be found in Fig. 14b. However, it has to be realised that the intervals do not begin at point in time 0, as initially the response is still in the elastic phase. To the deflection w_{max} at t_{max} applies:

$$w_{max} = \frac{\hat{v}}{2} t_{max} = \frac{M_e \hat{v}^2}{2F_p} = \frac{3}{128} \frac{(\hat{f} t_d l)^2}{\varrho A M_p} \tag{50}$$

The normalized quantities w_{max} and τ_{max} have been computed for the cases VEG5P5 to VEG5P2 inclusive and for VEG4P4 to VEG4P2 inclusive, based on the normalised values for the length l, the bending stiffness EI, the load $\hat{f}$ and the specific mass $\varrho(\varrho A = \pi^2/4)$ as used in this study. The values of the input quantities M_p and τ_d, as well as the results, are given in Table 12. As a result of the choice of ϱA, the fundamental tone is equal to 1 and therefore: $t_d = \tau_d$.

Table 12. Maximum plastic deflections and time intervals according to the computations with the single degree-of-freedom system. All quantities are dimensionless (see Chapter 2)

case	τ_d	M_p $(\cdot 10^{-3})$	F_p $(\cdot 10^{-3})$	$\hat{v}$ $(\cdot 10^{-3})$	τ_{max}	w_{max} $(\cdot 10^{-3})$
VEG5P5	0.01	2.885	11.54	3.040	.2167	.3293
VEG5P4	0.01	2.308	9.232	3.040	.2708	.4117
VEG5P3	0.01	1.731	6.924	3.040	.3611	.5489
VEG5P2	0.01	1.154	4.616	3.040	.5417	.8234
VEG4P4	0.10	17.18	68.72	30.40	.3639	5.531
VEG4P3	0.10	12.89	51.56	30.40	.4849	7.371
VEG4P2	0.10	8.590	34.37	30.40	.7275	11.06

The values of τ_{max} and w_{max} from the numerical computations are given in Table 13 below.

Table 13. Maximum plastic deflections and time intervals according to the numerical computation of the discrete model.

case	τ_{max}	w_{max} $(\cdot 10^{-3})$	$\hat{w}_{el}$ $(\cdot 10^{-3})$	w_{pla} $(\cdot 10^{-3})$
VEG5P5	.3285	.505	.256	.248
VEG5P4	.3560	.570	.218	.352
VEG5P3	.4280	.680	.167	.513
VEG5P2	.5975	.931	.109	.822
VEG4P4	.4360	6.43	1.57	4.87
VEG4P3	.5735	8.15	1.24	6.90
VEG4P2	.7925	11.6	.824	10.7

When Tables 12 and 13 are compared both similarities and differences are found. Characteristic is the larger similarity of the maximum deflections observed in both theories, with increasing ductility at midspan. This agrees with expectations. With a larger plastic rotation in the middle of the beam this type of deformation becomes more and more dominant compared with the more complicated behaviour in the initial phase of the response.

The maximum deflections computed with both theories, show one systematic difference. This difference is the neglect of the amplitude of the remaining elastic vibration in the rigid plastic single degree-of-freedom system. These amplitudes are given in Table 13 in the column headed $\hat{w}_{el}$. There is a clear tendency that a larger energy

dissipation by plastic rotations leads to a smaller amplitude of the remaining elastic vibration. When the amplitude is subtracted from the maximum deflection, the result is the permanent deflection, in the table denoted by w_{pla}.
A comparison between w_{max} of the rigid-plastic single degree-of-freedom system and w_{pla} from the numerical solution of the discrete model shows that the values of the permanent deflections are nearly the same in the cases with a plastic moment of 20% of the maximum occurring elastic moment. With the shortest load duration the difference between the methods is only 0.23 percent. The somewhat longer load duration results in a difference of 3.0 percent. With a plastic moment of 30 percent of the elastic value the permanent deflections of both load durations correspond reasonably well. The differences are around 7 percent. In the cases with a 40 percent plastic moment, when there is again a lower amount of plastic deformation, it can only be said to be in the same order of magnitude. Then the differences have increased to 17 and 14 percent for τ_d values of 0.01 and 0.10 respectively. When the level of the plastic moment increases to 50 percent, the permanent deflection computed with the single degree-of-freedom system is 33 percent higher than that of the discrete model. In that case, the assumption of a dominant plastic hinge in the middle of the field is apparently no longer valid. A significant part of the initial kinetic energy is dissipated in zones close to the supports. The values of τ_{max} can be compared as follows. The starting point of the plastic periods of the middle cross-section in the numerical computations can be derived from the time plots of the bending moments or the plastic deformations (for example from Fig. 14b). These starting points can be subtracted from the τ_{max} of the numerical solution. The starting points and the recalculated values of τ_{max} are given in Table 14. This results in a better assessment of the single degree-of-freedom system in relation to the numerical solution. The accuracy of the determination of the τ_{max} with the single degree-of-freedom varies from acceptable to good.

Table 14. Recalculation of the plastic periods for a better comparison with the single degree-of-freedom system.

		τ_{max}	
case	start pl. per.	numerical	degree-of-freedom system
VEG5P5	.0865	.242	.217
VEG5P4	.0650	.291	.271
VEG5P3	.0635	.365	.361
VEG5P2	.0650	.533	.542
VEG4P4	.0945	.342	.364
VEG4P3	.0880	.486	.485
VEG4P2	.0795	.713	.728

Also the dynamic support reaction can be determined with the single degree-of-freedom system. In the numerical simulation the dynamic support reaction is not determined explicitly, but it is about equal to the shear force in the cross-section nearest to

the support. Fig. 14b clearly shows that the variation with time of the shear force in the initial phase is equal to the elastic case. This is logical, since plastic deformations do not yet occur in that phase. It is clearly visible that shear forces strongly decrease in value in the plastic phase and have a more or less constant value. This is in accordance with the moment distribution remaining more or less constant during the plastic yielding.
In setting up the model, the deflection at the middle of the field was chosen to be the characteristic parameter. The internal force of this model is related to the bending (plastic) moment in the middle of the beam. Therefore the plastic "spring force" F_p cannot be used to determine the dynamically occurring support reaction. A dynamic equilibrium equation has to be formulated from which the dynamic support reaction can be determined. In this equation the external load, the support reactions and the inertial force of the model form an equilibrium of vertical forces. The distribution of the inertial forces along the beam is identical to the deflection, i.e. linearly increasing from the supports towards the middle of the field. If the maximum inertial force per unit length in the middle of the field is equal to $\hat{F}_i$, it can be derived from:

$$\hat{F}_i = \frac{F(t) - F_p}{M_e} = 3\,\frac{F(t) - F_p}{\varrho A l} \tag{51}$$

$F(t) = \frac{1}{2} l f(t)$ being the equivalent load. The equivalent load produces the same amount of external work as the actually present uniform load. In the formulation of the equilibrium equation, the real load is again taken into account, based on the now determined acceleration. The equilibrium equation is:

$$R(t) = \frac{l f(t)}{2} - \frac{\varrho A l F_i}{4} \tag{52}$$

After further substitution of the acceleration $\hat{F}_i$ and the definitions of F_p and $F(t)$ used here, it follows that:

$$\begin{aligned} R(t) &= F(t) - \frac{3}{4}\left(\frac{F(t)}{2} - F_p\right) \\ &= \frac{F(t)}{4} + \frac{3}{4} F_p \end{aligned} \tag{53}$$

The time plot of the dynamic support reaction is therefore of the same form as the load, superimposed to a constant value. The formula can also be written as:

$$R(t) = 0.125 \hat{F}\,\frac{\max\,(t_d - t, 0)}{t_d} + \frac{3M_p}{l} \tag{54}$$

The reaction for an explosion load has a maximum at $t = 0$. This maximum is called R_{piek}. Following the positive phase length, the support reaction remains constant as long as yielding occurs in the middle cross-section. This constant value is called R_{const}. In the numerical computations it takes some time before the plastic phase begins. As a result, the high shear force peak from the other end of the beam has already reached

the support under examination, before the plastic phase gets a chance to attenuate the propagating waves. The numerical results may show more peaks in the shear force or support reaction than in the single degree-of-freedom system.
The results of the single degree-of-freedom system are given in Table 15. The peak values of the numerical computations are also given in this table. For two illustrative cases, the constant values of the support reaction have been shown in the time graphs of the shear force. These can be found in the Figs. 14 and 22. The correlation appears to be very good.

Table 15. Dynamic support reactions in the rigid-plastic single degree-of-freedom system and the beam model denoted with TILLY (explanation of the names: see previous page)

case	R_{piek} $(\cdot 10^{-3})$	R_{const} $(\cdot 10^{-3})$	$R_{piek,TILLY}$ $(\cdot 10^{-3})$
VEG5P5	134	8.77	26.4
VEG5P4	132	7.02	26.4
VEG5P3	130	5.26	26.4
VEG5P2	129	3.51	26.4
VEG4P4	177	52.2	117
VEG4P3	164	39.2	117
VEG4P2	151	26.1	99.5

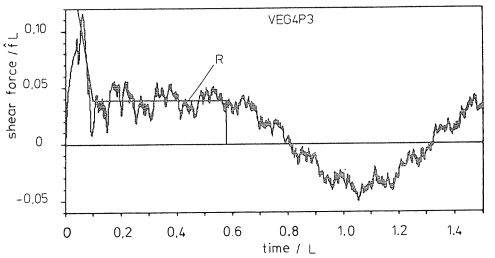

Fig. 22. Time plot of the shear force close to the support in the case VEG4P3.

7 Results of the investigations (hardening)

After the examination of the influence of elasto-plastic behaviour of the cross-section, on the response of the beam and the distribution of the occurring plastic rotation along the beam, the question arose whether it should be possible to locally undergo this strongly concentrated plastic deformation. Another question is, to what extent this concentration is sensitive to variation of the properties that have already been introduced and to addition of properties that previously were not taken into account. One of the properties that has not yet been introduced is the occurrence of hardening. In the M-$\varkappa$ diagram, hardening is expressed by a certain percentage of remaining stiffness after the plastic area has been reached (see Fig. 23).

In this chapter it will be explained what hardening is understood to be and which input quantities of the numerical model have been adapted in relation to the elasto-ideal-plastic model. The bending springs are replaced by two parallel springs, namely one elastic and one elasto-plastic spring. Then the results will be described. Finally some conclusions are drawn.

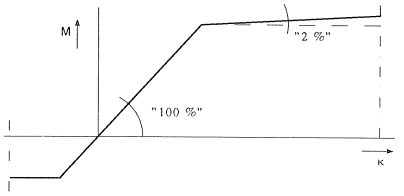

Fig. 23. Definition of the percentage of hardening. The hardening percentage is 2 percent.

7.1 *Hardening*

In the previous paragraph the phenomenon of hardening in concrete beams is mentioned. The decrease of the height of the concrete pressure zone, which is coupled with an enlargement of the internal lever arm, causes an increasing bending moment, also during the yielding of the mild steel. When pre-stressed with steel or aramide the hardening is probably caused by the prestressing.
The value of the hardening is expressed as a percentage of remaining stiffness after yielding, in relation to the initial stiffness. This is explained in more detail in Fig. 23.
As a result of this increasing bending moment in a cross-section, more energy is needed to cause a certain amount of plastic rotation. Another result is that the adjacent cross-sections of the beam are more heavily loaded than would have been the case with ideal-plastic yielding of the cross-section. These two phenomena give rise to the expectation that the presence of hardening in the yielding branch causes the maximum ductility demand in the beam to be smaller than with an ideal plastic yielding branch under identical conditions.
So, when the ductility demands of the elasto-ideal-plastic properties of the beam have been established, it is interesting to quantitatively examine the influence of hardening. In this study, percentages of hardening of 2 and 5 were chosen. Especially the latter value is rather large for practical conditions. For example, with a ductility demand of 20 the increase of the bending moment is identical to the original plastic moment.
For reinforced concrete this can no longer be called realistic. However, when the concrete is reinforced or pre-stressed with aramide fibres such values of hardening may certainly occur. To examine the influence of hardening, the value of 5 percent in any case can be used as an upper limit for the determination of the influence of hardening on the distribution and the maximum value of the ductility demand.

7.2 *Quantification of the hardening model*

The influence of hardening has been examined for all cases computed in the previous chapter with $\tau_d = 0.01$ and $\tau_d = 0.1$ (VEG5P5 to VEG5P2 inclusive and VEG4P4 to VEG4P2 inclusive). In all these cases a hardening percentage of 2 was applied and for the cases VEG5P5 to VEG5P2 a percentage of 5 was also included in the computations. In the nomenclature a digit was added to distinguish the various computed beams. This digit is 2 for the computations with a hardening of 2 percent and 5 for the computations with a percentage of 5. So the code VEG5P32 means: simply supported, uniformly distributed explosion load, $\tau_d = 0.01$, plastic moment 30 percent, hardening 2 percent.
The elasto-plastic spring with hardening was not included in the version of the TILLY program used. Therefore, the bending behaviour has been schematically represented in the model using two springs linked in parallel. One elasto-plastic spring (EP spring) provides for the discontinuity in the moment-curvature diagram and a linear-elastic spring (LE spring) adds to the model the stiffness that remains present during the plastic phase. This combination of springs is to provide the same value of the plastic moment and the same yield curvature as in the elasto-plastic cases.
In Table 16, the values of the spring stiffness and the yield force in the springs that describe the bending, are given for the cases that were computed. It has to be kept in mind that for the determination of the bending moments, an arm of 1/20 of the span applies. In all computations an element distribution of 20 elements per half beam length has been used.

Table 16. Plastic moments and stiffness of the computed elasto-plastic beams with hardening (explanation of the nomenclature see paragraph 7.2)

	yield strength EP spring	stiffness EP spring	stiffness LE spring
VEG5P52	.05655	31360	640
VEG5P42	.04524	31360	640
VEG5P32	.03393	31360	640
VEG5P22	.02262	31360	640
VEG5P55	.05482	30400	1600
VEG5P45	.04385	30400	1600
VEG5P35	.03289	30400	1600
VEG5P25	.02193	30400	1600
VEG4P42	.3367	31360	640
VEG4P32	.2525	31360	640
VEG4P22	.1684	31360	640

7.3 *Results*

The results of the 11 computations carried out are given analogous to the previous chapter, to enable a good comparison with the computations in the elasto-ideal-plastic domain. First the occurring deflections are compared. Next, diagrams have been made

showing the occurrence of plastic yielding along the beam with time. The distribution of the maximum ductility along the beams is presented graphically. Also Q-μ diagrams were made to illustrate the occurring combinations of shear force and plastic rotations (expressed in ductility).

Deflections

The maximum and permanent deflections w_{max} and w_{pla} of all elasto-plastic computations are given in Table 17. The permanent plastic deflection is determined as being the average of the maximum and the minimum deflection after yielding.

It is clearly visible that both the occurrence of hardening and the percentage of hardening considerably influence the decrease of both the maximum and the permanent deflection in the middle of the span. The amplitude of the remaining elastic vibration continuously decreases with decreasing hardening and increasing plastic rotation.

Table 17. Maximum and permanent deflections of all elasto-plastic beams, computed with several percentages of hardening

	w_{max} $(\cdot 10^{-3})$			w_{pla} $(\cdot 10^{-3})$		
hardening	0%	2%	5%	0%	2%	5%
VEG5P5	.505	.494	.485	.248	.234	.216
VEG5P4	.570	.547	.534	.352	.314	.289
VEG5P3	.680	.641	.615	.513	.448	.402
VEG5P2	.931	.819	.756	.822	.668	.568
VEG4P4	6.43	5.89	-	4.87	3.97	-
VEG4P3	8.15	7.06	-	6.90	5.45	-
VEG4P2	11.6	9.22	-	10.7	7.91	-

Yielding areas

Especially for the weakest beam, two things become clear regarding the occurrence of yielding along the beam with time. With an increasing percentage of hardening, the duration of the plastic phase is shorter and a larger part of the beam is involved in the plastic rotation. The strong concentration of plastic rotation in the middle of the beam in the ideal-plastic case, occurs to a much lesser extent in this case. In the beam with a 50 percent plastic moment the influences of hardening are hardly noticeable.

Ductilities

In the distribution of the maximum ductility demands along the beam axis, the tendency to de-concentration of plastic rotation is clearly visible too. Also the values appear to have strongly decreased compared with the elasto-plastic situation without hardening. The beam with a 20 percent plastic moment has maximum ductility demands of 37.1, 9.1 and 7.3 for percentages of hardening of 0, 2 and 5 respectively. This arouses the suspicion that the presence of hardening is more relevant to the spread of the plastic rotations than the actual percentage.

The graphs of the computations with a 2 percent hardening are given in Fig. 24. A comparison of this figure with the Figs. 17 and 19 shows, apart from the large decrease of the plastic rotation in the middle, a widening of the plastic zones.

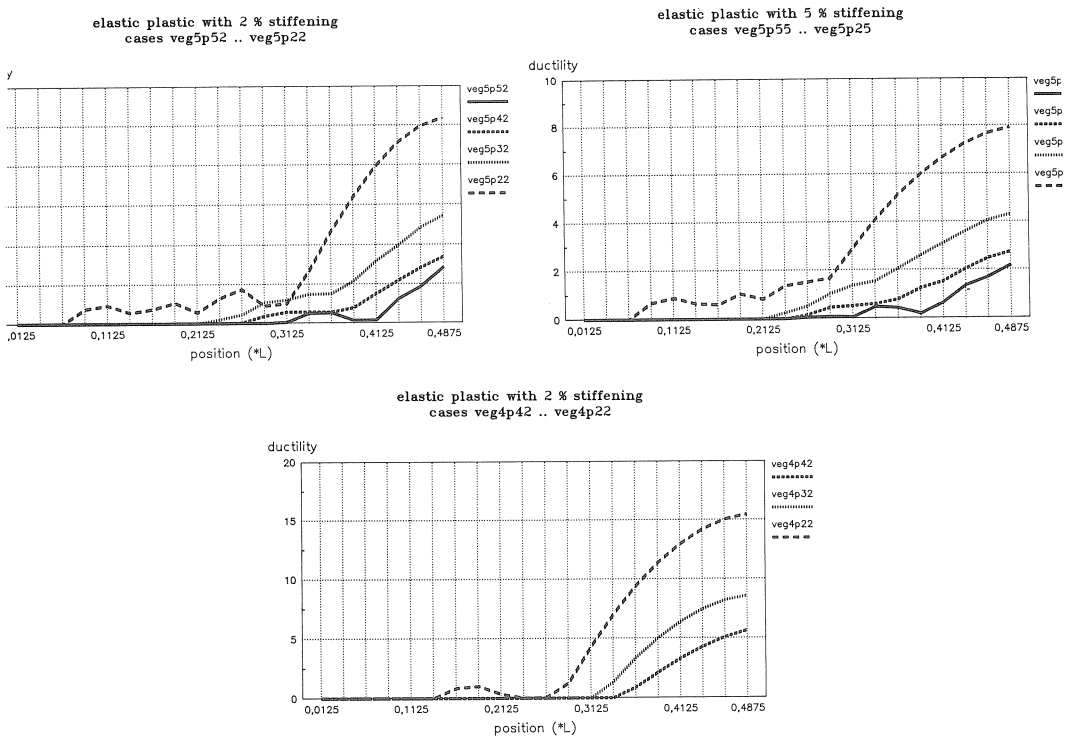

Fig. 24. Ductility distribution along the beam (VEG5P52 to VEG 5P22 inclusive, VEG5P55 to VEG5P25 inclusive and VEG4P42 to VEG4P22 inclusive).

The influence of the hardening is even more striking at $\tau_d = 0.1$. Then, in the weakest beam the ductility is reduced from 85.9 to 14.2.

It has to be stated that the graphs are based on the plastic deformations as they occur at point in time $\tau = 1$. Because of the possible occurrence of negative plastic deformations this does not have to result in the maximum values of the ductility demands.

The ductility demands can be integrated over the entire beam, to gain an impression of the influence of hardening on the overall ductility demand. The results of the summations of all elasto-plastic computations are given in Table 18. In setting up this table the actual maximum ductility demands were taken into account and not those at point in time $\tau = 1$. The overall ductility appears to decrease slightly with increasing hardening. As was to be expected, the increased capacity to store elastic deformation energy, causes a decrease in the required energy dissipation by plastic deformation. Indeed more elastic deformation energy can be stored. It should be kept in mind that, with a ductility demand of for example 10 with a hardening of 2 percent, the increase of the bending moment in the cross-section in relation to the plastic moment is 20 percent.

Table 18. Overall ductility demands of all elasto-plastic beams, computed with various percentages of hardening

	positif overall duct		
hardening	0%	2%	5%
VEG5P5	7.50	7.37	7.25
VEG5P4	13.47	12.87	12.64
VEG5P3	27.08	25.55	24.46
VEG5P2	66.53	60.60	56.81
VEG4P4	23.68	21.48	-
VEG4P3	44.62	40.46	-
VEG4P2	106.81	93.27	-

8 Simulated experiments

So far it has been the objective of this study to gain a theoretical understanding of the potential and the phenomena that occur in a discrete beam model under an explosion load and an impact (concentrated) load. However, it is important to know whether the elasto-plastic model, which was used all the time, can be validated with experimental results.
The simulation of experiments may often lead to complications, namely which phenomena and properties are normative and should be taken into account in the computing model. The temptation to do "curve fitting", by putting in tuning parameters, has to be resisted. Taking a priori assumptions as a starting point, the results have to indicate the validity of the model. Only in this way the model under examination can inspire trust, which enables it to be used, for example to predict the behaviour of structures.
It has been decided to simulate three experiments with the TILLY program, focusing on experiments in which the load is extended into the plastic area and which were well documented.

8.1 *Falling beams (ETH); description of the experiments*

In 1978, at the "Institut fur Baustatik und Konstruktion" of the "Eidgenossische Technische Hochschule" (ETH) in Zurich, a series of tests were started, called: "Versuche an Stahlbeton- und Spannbetonbalken unter stossartiger Beanspruchung". The tests were carried out by Amman and others, see references [16], [17], [18] and [19]. The objective of the tests was to gain more understanding of the behaviour of concrete under high loading rates and the corresponding energy absorption.
In the experiments both entire structures were tested and tensile tests were carried out with reinforcement steel and pre-stressed steel under various strain velocities. The tests on entire structures concerned falling beams on an elastic support and beams over more fields, with a suddenly failing support. For the study described in this report experiments with falling beams were chosen. A previous DIANA computation for this beam is reported in [20].

The beam is 8.15 m long, 0.40 m wide and 0.3 m deep, it is freely supported at one end and is able to rotate in the vertical plane. When in horizontal position, the other end rests on a shock absorber with a spring. With a crane this end can be lifted to the desired drop height. The span between the hinge and the shock absorber is 7.85 m. Fig. 25 shows the experimental set-up. The length-height ratio of this beam is about 26. This corresponds fairly well with the ratio of 20 in the VEG computations.

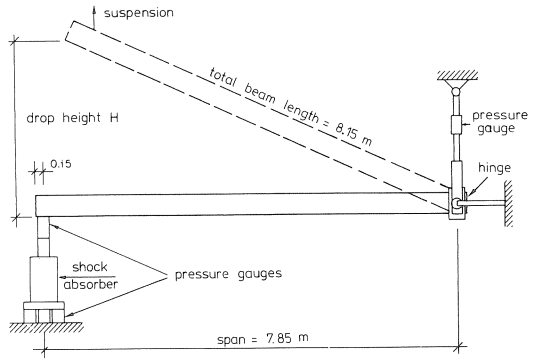

Fig. 25. Experimental set-up for a falling beam [17].

A linear, vertically directed velocity as well as a constant angular velocity develop along the beam axis after the beam is dropped. It was assumed that the deformation of the beam during the fall does not yet play a role in the development of the impulse. When the beam becomes horizontal, it hits the shock absorber which causes the velocity to be strongly diminished at that position. This results in the propagation of a bending wave and a shear wave into the beam from the shock absorber.
After a short period of time a maximum deflection and bending moment will develop at about 40 to 50 percent of the beam length, measured from the shock absorber. In the experiment the plastic moment was exceeded in many places, with maximum plastic rotations at a distance of about $0.43l$ from the shock absorber.
In this study experiments with three beams are simulated. These are denoted B1, B8 and B13. The main difference between these beams is the type and the percentage of the reinforcement. The beam B1 was tested once, the others were subjected to a drop several times. Only the first drop of each beam has been simulated in this study. The results for beam B1 were also presented at the IABSE colloquium in Delft in 1987 [26]. The Young's modulus of the concrete used, is not stated explicitly in the reports. In [17] it is advised to follow the dynamic Young's modulus in accordance with the formula:

$$E_c' = 1900\sqrt{10 f_{cw}} \tag{55}$$

The following properties were used in the TILLY computations:
all beams: - beam size: cross-section 0.4 m × 0.3 m
length: 8.15 m
span: 7.85 m

B1:	- reinforcement:	$\omega_0 = 0.56\%$; $\omega_b = 0.21\%$
	- reinforcement steel:	hot rolled
	- tensile strength steel:	$f_{st} = 550$ N/mm^2 (static)
	- compressive strength concrete:	$f_{ccm} = 46.0$ N/mm^2 (static)
	- tensile strength concrete:	$f_{ctm} = 3.30$ N/mm^2 (static)
	- beam mass:	300 kg/m
	- shock absorber:	spring buffer
	- drop height:	$H = 3.75$ m
B8:	- reinforcement:	$\omega_0 = 1.07\%$; $\omega_b = 0.20\%$
	- reinforcement steel:	hot rolled
	- tensile strength steel:	$f_{st} = 559$ N/mm^2 (static)
	- compressive strength concrete:	$f_{ccm} = 42.4$ N/mm^2 (static)
	- tensile strength concrete:	$f_{ctm} = 3.12$ N/mm^2 (static)
	- beam mass:	300 kg/m
	- shock absorber:	shock damper
	- drop height:	$H = 3.75$ m
B13:	- reinforcement:	$\omega_0 = 0.34\%$; $\omega_b = 0.22\%$
	- reinforcement steel:	pre-stressing steel 950/1150
	- tensile strength steel:	$f_{st} = 952$ N/mm^2 (static)
	- compressive strength concrete:	$f_{ccm} = 43.7$ N/mm^2 (static)
	- tensile strength concrete:	$f_{ctm} = 3.18$ N/mm^2 (static)
	- beam mass:	300 kg/m
	- shock absorber:	spring buffer
	- drop height:	$H = 1.30$ m

In fact the beams B1 and B8 are completely identical (also the same drop height), except for the percentage of reinforcement at the bottom of the beam. This is about twice as much in beam B8 than in beam B1 so that the plastic moment is about twice as large. In beam B13, on the contrary, the percentage of reinforcement is smaller than in beam B1, but a different type of steel, with a higher yield stress, was used so that about the same plastic moment is reached as in beam B1. However, this pre-stressing steel has a much smaller rupture strain than hot rolled steel. For this reason the drop height was chosen significantly smaller. The compression of the shock absorber appeared to be small in relation to the maximum deflection of the beams. Therefore the influence of the shock absorber is negligible and also the type of shock absorber is of no importance.
The influence of the maximum strain rate on the properties of the concrete and the steel were taken into account, in the determination of the cracking moment and the plastic moment. The strain rates of the concrete, measured in the tensile zone, are in the order of 0.01/s. For the splitting strength of the concrete, the corresponding dynamic enlargement factors of 1.4 are used. The enlargement factors for the steel are assumed to be 1.15 for B1 and 1.10 for the other two beams. The establishment of these factors was based on the strain rates measured during the experiments. These velocities are shown in the Figs. 26 and 27. Such an enlargement factor can also be determined

for the compressive strength of concrete. This has, however, not been done in these computations, as only the cracking moment and the plastic moment together with the corresponding curvatures are required for the description of the properties of the bending springs. It is not intended to simulate the collapse of the compressive zone of concrete. The response is computed up to the phase in which no new plasticity occurs. In retrospect it can be checked whether the rotation capacity or the permissible ductility μ_u is not exceeded.

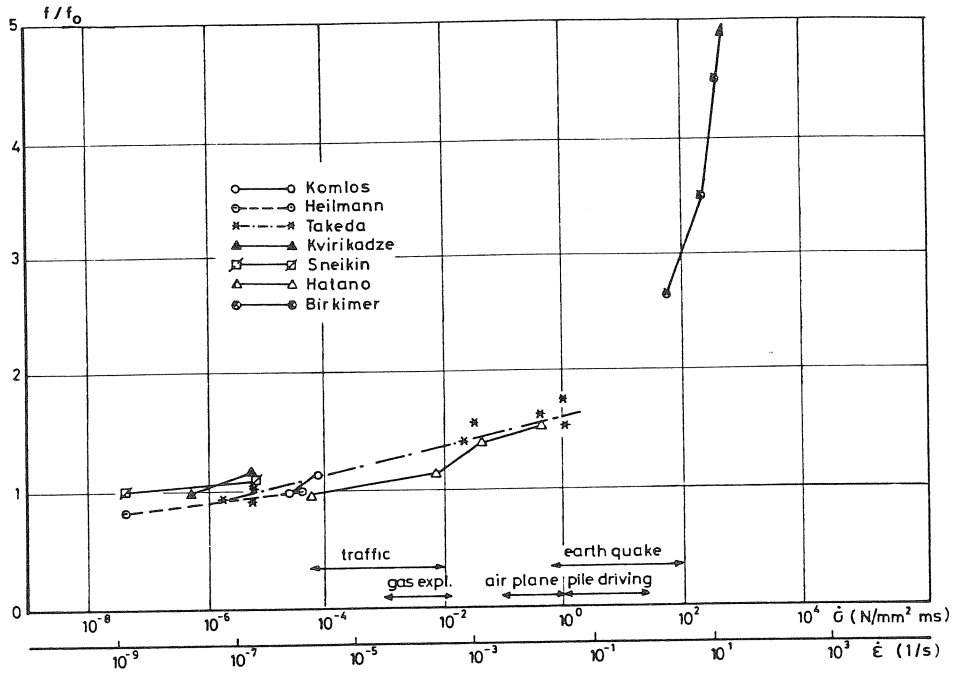

Fig. 26. Dependence of the splitting strength of concrete on the strain rate [30].

Table 19 shows the chosen material quantities as well as the resulting values of the cracking moment M_{cr}, the plastic moment M_{sy} and the ultimate failure moment M_u, with the corresponding curvatures, for all three beams. For the M_u also the corresponding rotation ϕ_u of the bending spring in the TILLY model is given.
Finally the percentage of hardening was determined from the applied moments and curvatures using the equation:

$$\text{hardening } \% = \frac{(M_u - M_{sy})\varkappa_{sy}}{M_{sy}(\varkappa_u - \varkappa_{sy})}$$

This percentage has not been included in the present computations.

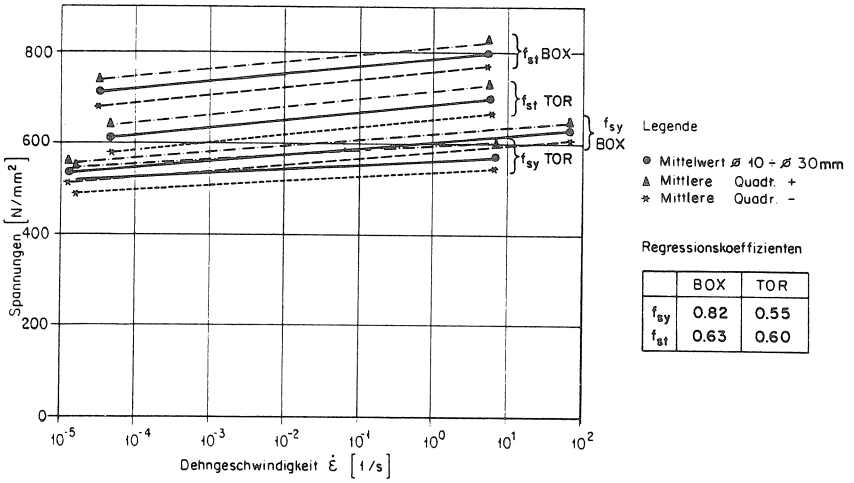

Fig. 27. Dependence on the yield strength of steel on the strain rate [16].

Table 19. Material quantities and resulting values for moments and curvatures of 3 falling beams

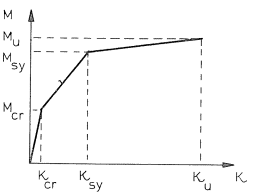

	B1	B8	B13
f_{ctm}^{dyn} (N/mm²)	4.6	4.3	4.5
f_{ccm}^{dyn} (N/mm²)	59.8	55.1	56.8
f_{st}^{dyn} (N/mm²)	640	620	1040
E_c^{dyn} (N/mm²)	39800	38200	38800
E_s^{dyn} (N/mm²)	210000	210000	210000
M_{cr} (kNm)	35.0	33.2	33.8
$\varkappa_{cr}$ (10^{-3} m^{-1})	0.98	0.97	0.96
M_{sy} (kNm)	96.4	170	93.4
$\varkappa_{sy}$ (10^{-3} m^{-1})	14.5	15.6	21.3
M_u (kNm)	99.5	172.1	94.9
$\varkappa_u$ (10^{-3} m^{-1})	116	58.2	116
ϕ_u (10^{-3})	46.3	24.6	50.0
μ_u	7.0	2.7	4.4
hardening %	0.46	0.47	0.38

The numerical values in the Figs. 28, 29 and 30 have been taken from [21] and show the reinforcement distribution of the three beams and the M-$\varkappa$ diagram. The shaded areas in the figures denote the amount of energy dissipated in the cracks of the cross-section. It is clearly visible that this energy varies considerably with the different beams, but it is always small compared to the total energy dissipation at the maximum plastic rotation.

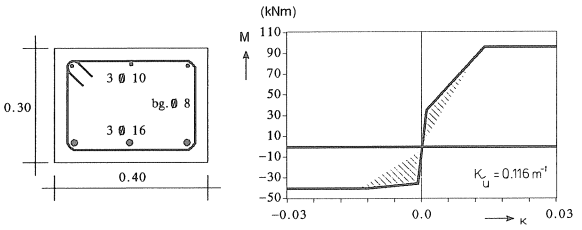

Fig. 28. Cross-section and moment-curvature diagram of beam B1.

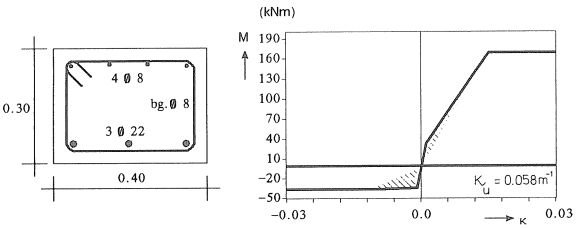

Fig. 29. Cross-section and moment-curvature diagram of beam B8.

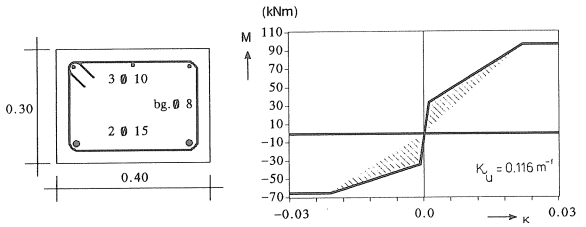

Fig. 30. Cross-section and moment-curvature diagram of beam B13.

The value of the maximum occurring deflection and the point in time of the occurrence can be calculated by hand with a schematic representation into a single degree-of-freedom system, using the method described in the chapter concerning the elasto-plastic results.

Now it is important to know the initial velocity of the beam when it hits the shock absorber. A simple equation of the potential energy of the beam shortly before release, and of the kinetic energy in the horizontal position shortly before it hits the shock absorber leads to the value of the velocity of the left side of the beam:

$$\int_0^l \frac{1}{2} \varrho A v^2(x)\, dx = \int_0^l \varrho A g h(x)\, dx \tag{56}$$

in which g is the gravitational acceleration, $v(x)$ the velocity and $h(x)$ the drop height. The height of the beam is neglected in relation to the length, The drop height $h(x)$

decreases linearly from h_0 to zero. Also the velocity decreases linearly from v_0 at $x = 0$ to zero at $x = l$. Working out (56) results in:

$$v_0 = \sqrt{3gh_0} \tag{57}$$

The initial velocity distribution could also originate from an identically distributed transient load. From a static computation of the moment line, resulting from such a linear varying load, it follows that the maximum bending moment is at $x = 0.423l$. In this the weight of the beam is neglected. With a static distribution of forces, this is the position where the plastic hinge develops and where the falling beam has an initial velocity of $0.577v_0$. At the point in time when the beam hits the shock absorber, impulses are applied to the beam via the supports, which change the initial velocity of the beam at $x = 0.423l$ from $0.577v_0$ to $0.789v_0$. This velocity is called $\hat{v}$. The plastic resistance force now reads:

$$F_p = \frac{4.206M_p}{l} \tag{58}$$

When, subsequently, the values of F_p and $\hat{v}$ in the expressions (49) for t_{max} and (50) for w_{max} are substituted for the beams B1, B8 and B13, M_e still being (46), this results in the values shown in Table 20. It has to be remembered that w_{max} should actually be regarded as the permanent or plastic deflection.

Table 20. Results of computations by hand for three falling beams.

	t_{max} (s)	w_{max} (s)
B1	.166	.687
B8	.083	.342
B13	.097	.237

8.2 *Discrete models of the beams*

For the schematic representation of the beam as a discrete model, the beam has been divided into 20 elements. These elements are mutually linked by bending and shear springs. In the elements both the translation inertia and the rotation inertia are schematically represented as masses. This means that the Timoshenko beam is modelled. The exact positions of the degrees-of-freedom and the springs as well as the entire model are shown in Fig. 31.

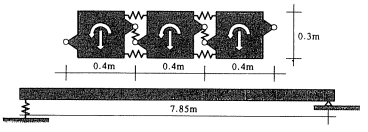

Fig. 31. The schematic representation of the falling beam.

Initially, three linear-elastic computations were carried out, with the objective to establish the magnitude of the bending moment under these conditions. This has been done to determine in advance whether these tests can be compared to the cases considered previously in this study, in which the plastic moment was chosen as a percentage of the largest elastic moment.
With linear-elastic behaviour of the cross-section, the maximum bending moments occur in the cross-sections 14 (beam B1 an B8) and 13 (beam B13). Cross-section 13 is situated at $0.63l$ of the shock absorber and cross-section 14 at $0.68l$. The values as well as the plastic moments and the percentages are given in the table below. At position $0.43l$ the maximum bending moments are not much smaller.
The percentages of the plastic moments are all under 30, see Table 21. For B1 the percentage is almost as low as 20! So, the tests do correspond with the lowest percentages that were previously examined. In view of the experience gained from the examination of the elasto-plastic beams, this arouses the expectation that a large and concentrated plastic rotation will occur near the middle of the span.

Table 21. Percentages of plastic moments of the three simulated experiments

	$M_{max,el}$ (kNm)	M_p (kNm)	percentage (%)
B1	460.9	96.4	20.9
B8	619.5	170.0	27.4
B13	362.4	93.4	25.8

Now the problem arises how to model the real behaviour of the cross-section of a beam. The objective is to simulate the experiment sufficiently accurately. A model is always an idealized reality and the question is whether certain physical phenomena that occur are excluded by this idealization. Initially it was tried to describe the cross-sectional behaviour with one elasto-plastic bending spring. The contribution of the concrete in the tensile zone (tension-stiffening) is then neglected and from the start the stiffness of the bending spring is identical to that of the cracked cross-section, integrated over the element length between the springs. It is clear that this concurs with the elasto-plastic study described in the previous chapters and that the realism of the elasto-plastic model is tested. Hereafter the computations with this model will be called "TILLY-EP".
Another model is also used. In the final phase of the investigation, Sluys added a new type of spring to the TILLY program, to more accurately describe the moment-curvature diagram under cyclic loading conditions [21]. For this the model developed by Takeda has been used. It will be called the "cycle-model" (Dutch: "wissel-model"). This element intends to describe the real moment-curvature diagram, including the realistic unloading branches and the occurring hysteresis. However, the cyclic model cannot describe hardening. Whether and to what extent the stiffness has to be adapted, is considered at every time step on the basis of the plastic history. Also the tension-stiffening effect of the influence of cracking on the spring stiffness, is computed more effectively with this element. The computations carried out with this model will be called "TILLY-WISSEL"

8.3 *Results*

The computations of the three beams have been carried out with the two models described (time step = 0.0001 s) and the results of the deflection with time at about 0.43*l* of the shock absorber are given in the Figs. 32 to 34 inclusive.
Both the elasto-plastic "TILLY-EP" model and the complicated "TILLY-WISSEL" model give a good approximation of the maximum deflection. This means that the simple bi-linear diagram used in the previous chapters is very suitable.
The "TILLY-WISSEL" model is much more suitable to describe the behaviour of the remaining vibration after the occurrence of the maximum.

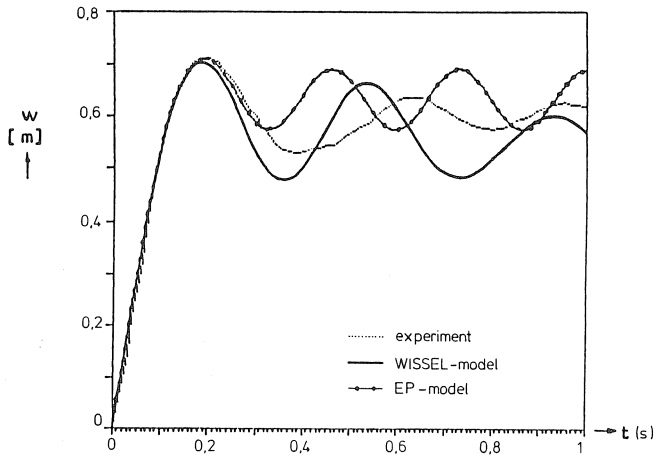

Fig. 32. Time plot of the deflections at position 0.43*l* of beam B1, according to the experiment and to the "TILLY-EP" and "TILLY-WISSEL" computations.

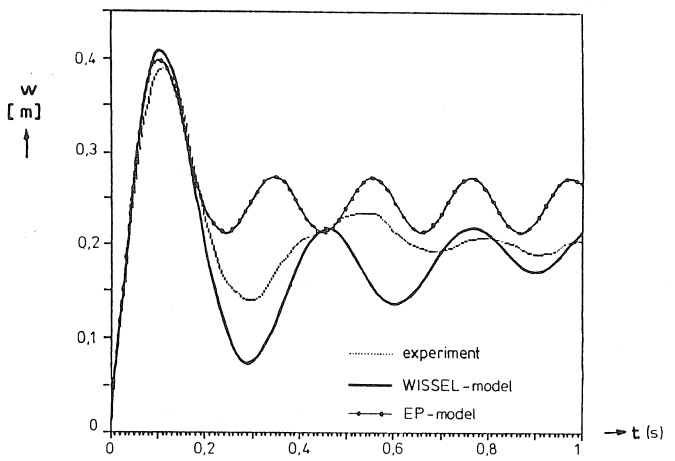

Fig. 33. Time plot of the deflections at position 0.43*l* of beam B8, according to the experiment and to the "TILLY-EP" and "TILLY-WISSEL" computations.

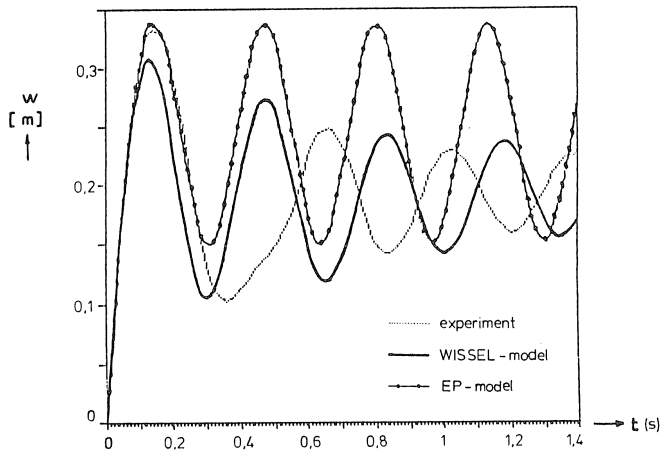

Fig. 34. Time plot of the deflections at position 0.43l of beam B13, according to the experiment and to the "TILLY-EP" and "TILLY-WISSEL" computations.

The experiments clearly show damping and so does the hysteretical "TILLY-WISSEL" model. The bi-linear model "TILLY-EP" provides no damping at all and does react somewhat too stiff at this stage (too small period). It is, however, striking that for experiment B13 the description of the maximum displacement is again better with the simple model (TILLY-EP). The permanent deflection in the computations with the simple model (TILLY-EP), becomes larger than appears from the experiment.
All experiments show an irregularity in the graph during the first unloading cycle. At that point the half period is much larger than the ones that occur later. As none of the computing models shows this, there is a small permanent phase shift between the computational results and the experimental results. Slipping of the reinforcement at the second increase of the moment is a possible explanation.
Initially, the amount of damping determined from the time graph, using the logarithmic decrement, appears to be very large in the experiments. The ratio between the first and the second amplitude is large because of the phenomenon mentioned in the previous paragraph. This phenomenon has not been included in the TILLY model and explains the large differences. The amount of damping that belongs to the period at the most right of the time scale, is less influenced by possible slip and therefore a comparison between computation and experiment is easier. In the experiments with the beams B1, B8 and B13, the amount of damping is about 12 percent, 8 percent and 4 percent respectively. The amount resulting from TILLY-WISSEL is in the order of 7 percent, 9 percent and 4 percent respectively.
Table 22 shows the maximum and permanent deflections of the three experiments and the TILLY computations.
In beam B8 the upper reinforcement is relatively smaller than in beam B1. This causes the relatively large negative curvatures after the "positive plastic phase". This results in

the permanent curvature being much smaller than the maximum plastic curvature. A definition of the plastic and permanent curvature is given in Fig. 35.

Table 22. Maximum and permanent deflections of the three falling beams.

	B1		B8		B13	
	w_{max} (m)	w_{pla} (m)	w_{max} (m)	w_{pla} (m)	w_{max} (m)	w_{pla} (m)
experiment	.71	.59	.39	.20	.33	.19
TILLY-WISSEL	.70	.54	.41	.20	.31	.20
TILLY-EP	.67	.63	.39	.25	.31	.24

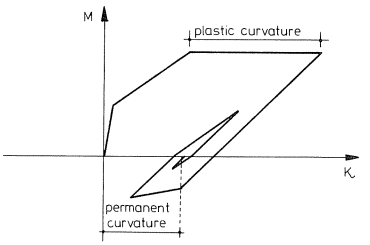

Fig. 35. Definition of the plastic and permanent curvature in the TILLY-WISSEL model.

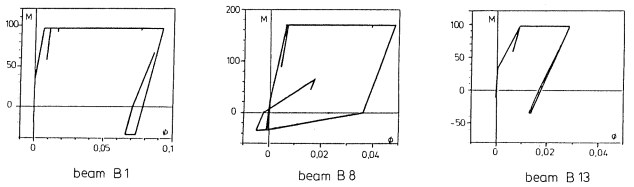

Fig. 36. Moment-rotation diagrams of a cross-section at the middle of the beam.

Fig. 36 shows some M-ϕ diagrams of computations of the TILLY-WISSEL model of cross-section 10 at position 0.48l, measured from the shock absorber.
In experiment B8 a large decrease of the permanent rotation is observed, which is absent in the other two experiments. This is caused by the fact that the negative cracking moment is already exceeded in the initial phase of the response. When the bending moment becomes negative again, the cross-section immediately becomes much weaker.
The Figs. 37, 38 and 39, show the computed and the measured curvatures. It is clear that the agreement between experiment and computation for beam B8 is poor. The beams B1 and B13 reflect the tendency of the experiment rather well, but the computed values are about 20 to 40 percent too high.

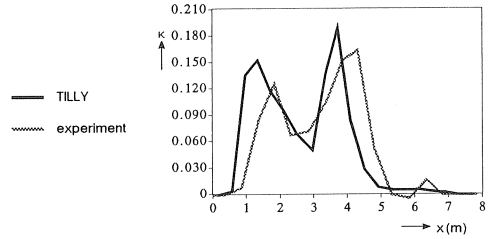

Fig. 37. Computed and measured permanent curvatures in experiment B1.

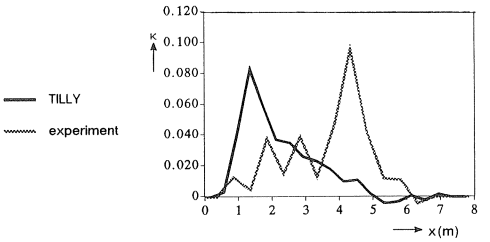

Fig. 38. Computed and measured permanent curvatures in experiment B8.

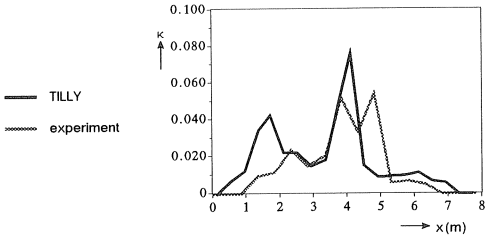

Fig. 39. Computed and measured permanent curvatures in experiment B13.

It has to be kept in mind that the Takeda model does not take hardening into account. Because of the hardening the maximum occurring plastic curvature is strongly reduced. It is not possible to predict whether the concurrence of the permanent curvatures will remain satisfactory, in a simple way.

The computations also allow for conclusions concerning the predicting value of the numerical analysis, whether or not bending will cause collapse (because the concrete pressure zone is crushed). The maximum rotation in the computation can be read from the moment-curvature history of the maximum loaded cross-section. In beam B1 that is $92.4 \cdot 10^{-3}$. The rotation capacity of the concrete spring, however, is $46.3 \cdot 10^{-3}$ (see Table 19). This agrees with a μ_u of about 7, as defined in this study.

The μ occurring in the computations is 15.5. This should lead to collapse of the compression zone. In the computation, however, hardening has not been included. In

Chapter 7 the influence of the percentages 0, 2 and 5 on the ductility demand were surveyed. The beam considered here has a hardening of 0.46 percent. The computations of Chapter 7 would show a reduction of the occurring μ of a factor of 2.4 with respect to 0 percent hardening. This factor reduces the ductility demand from 15.5 to about 6.5. Although this is smaller than μ_u, it is fairly well approximated. Experiment B1 indeed only showed slight damage of the concrete compression zone.
The maximum rotation of beam B8 is $48.6 \cdot 10^{-3}$. This is almost a factor of 2 larger than the rotation capacity, which is $24.6 \cdot 10^{-3}$. The percentage of hardening that could have been included in the calculation is 0.47 percent. Keeping in mind what was said before, this hardening would cause the maximum rotation to decrease with a factor of 2.4 and thus make it 10 percent smaller than the rotation capacity. In the experiment this beam locally failed to some extent in the compression zone.
The computation of beam B13 results in a maximum rotation of $41.2 \cdot 10^{-3}$, which is smaller than the rotation capacity $50.0 \cdot 10^{-3}$. Taking the hardening into account, the maximum rotation would be reduced by about a factor of 2. So no collapse is predicted. The first drop of this beam, which was tested repeatedly, did indeed not show any damage of concrete under compression.
The Swiss series of tests used a beam strongly resembling beam B1, in which the lower reinforcement, however, was reduced from 0.56 percent to 0.42 percent. This beam, denoted by B3, clearly began to fail. The cover in the compression zone was considerably crushed and the compression reinforcement buckled. The TILLY-WISSEL computation leads to $\mu = 30$ while $\mu_u = 9.8$. The percentage of hardening is 0.34 percent. This is too small to reduce the maximum ductility to such an extent that the cross-section is no longer in danger, for the reduction of μ with this percentage of hardening is smaller than 2. Therefore μ will certainly be 15, which is clearly larger than μ_u.
The predictive value of the computation model is clearly supported by all beams described here.

Conclusions

The computations of the falling beams show that the bi-linear elasto-plastic model used in this study, gives a good prediction of the maximum deflection and the point in time at which this occurs. Also the maximum occurring curvature can be predicted well if a small amount of hardening (in the order of 0.5 percent) is added.
The maximum occurring curvature in the computation is fairly realistic and can be used to predict whether or not the beam will fail in bending.
Concerning the behaviour of the remaining vibration, the simple bi-linear model is too simple. Therefore the estimation of the permanent curvature and the permanent deflection is too large.
The advanced cycle-model with hysteretic damping will have to be used in order to predict the behaviour of the remaining vibration well, i.e. the permanent curvature and the permanent deflection. With that the ultimate damping (in the order of 5 to 10 percent) during the remaining vibration will be described satisfactorily.

However, the deceleration in the response after the first reverse cycle cannot be explained by the cycle model.
The applicability of the models used in this study is stressed by the consideration that the modelling of the spring properties is based on design data without "curve fitting".

9 Conclusions

The subjects the conclusions apply to, are subdivided into two fields, namely elastic and elasto-plastic. The order of the conclusions is more or less based on the course of the description of the investigations.

9.1 *Linear-elastic computations*

1. It appeared that responses of beams, in which the behaviour is dominated by bending waves and shear waves, can be described with a discrete model consisting of masses and springs.
2. The choice of the element density is determined by the highest significant eigenmode. This will be higher with an increasing loading rate and concentration of the load. Also the type of support is important. The wave length of this significant eigenmode, consisting of a whole period, has to be divided into 6 elements or more.
3. The choice of the computation time step in the determination of the solution of the response, is determined by the highest eigenmode that can still be accurately solved. 1/5 of the eigenperiod of the highest eigenmode has to be taken as the upper limit of the time step. This rule should also be applied to elasto-plastic behaviour of the beam, since the highest eigenmodes still occur in the initial, elastic phase.
4. With increasing loading rate, the single mass-spring system first begins to fail for the shear forces, secondly for the bending moments and finally for the deflections. In this study the extent of the deviation for several cases is determined.
5. When the load becomes more geometrically concentrated, the single-mass spring system, as with the increasing loading rate, becomes less sufficient.
6. The distribution of reinforcement for dynamic loading is different from the distribution for static loading. More or less the same amount of reinforcement is needed over the whole length of the beam for bending. The same holds for shear reinforcement.

9.2 *Elasto-plastic computations*

1. When elasto-plastic behaviour is included, the ductility demand becomes more important in relation to testing against collapse criteria. The ductility demand is understood to be the occurring plastic deformation in relation to the maximum elastic deformation. Here this concept is used as a measure for the occurring damage that has to be compared to a maximum permissible ductility of the beam. The ductility demand concentrates at the middle of the span and increases progressively for smaller values of the plastic moment. The ductility demand also becomes larger when the load duration increases.

2. With elasto-plastic behaviour, the bending moment is obviously limited by the plastic moment used. Immediately after the load has been applied, the system remains elastic for some time. In that time interval the same shear forces occur as in the elastic computations. After the plastic hinges have been present for some time, the shear forces reduce strongly in magnitude and fluctuate around a constant value.
3. On the basis of the occurring combinations of shear force and ductility it can be concluded that in those cross-sections in which the ductility becomes larger than the order of 10, the simultaneously occurring shear forces have already decreased to a relatively small value. However, in many cases a significant ductility (μ in the order of 1) has already been reached with a shear force in the order of magnitude of the linear-elastic, i.e. relatively large, shear force.
4. The presence of hardening causes a redistribution of the occurring ductility and a strong decrease of its maximum value. The presence of any hardening is more important than the exact value of the percentage of hardening.
5. With the models used in this study it appeared to be possible to simulate experiments in which failure occurred due to bending. This proves the reality value of the model used. Here, input of some hardening is essential. The simulating potential for the shear forces has been proved less clearly, but there are enough indications to mark it sufficient.
6. The bi-linear elasto-plastic moment-curvature diagram used in this study has a good predictive value for the maximum deflection and the time in which it is reached. This model is too simple for the behaviour of remaining vibrations.
7. The input of a little hardening (in the order of 0.5 percent) causes a larger part of the beam to take part in the creation of the plastic hinge and gives a good approximation of the maximum occurring curvature with the elasto-plastic model. When the permanent plastic displacement and curvature have to be computed as well, a more accurate model will have to be used, which describes the behaviour under cyclic loading conditions better (hysteretic damping).
8. The maximum displacement and the time at which it occurs can be estimated with a single plastic degree-of-freedom system. This will be more accurate when the plastic moment is chosen to be smaller than the maximum bending moment that occurs under the same loading conditions with linear-elastic cross-sectional behaviour. When this percentage is in the order of 20 to 30, the results of this simple model may even be called very good. Concerning the support reaction this simple model gives too high peak values in the beginning, but a reliable order of magnitude for the average, constant value during the plastic phase.

9.3 *General*

Both for linear-elastic and elasto-plastic computations the discrete beam model of masses and springs is very suitable. The main advantage of this approach is that the computations can be carried out on a personal computer in times that can be kept under control (computing times often less than one hour per case), and at low costs. Therefore

it has been possible to consider a large number of combinations (about 70) of the chosen parameters. This should still to be considered impossible with an advanced element method package for problems of non-linear dynamics. With this type of investigation a PC environment is also very suitable to visualise the results. The beam model used has the advantage that the stress resultants (moment and shear force) that are familiar to the designers are immediately supplied as output. The results confirm the practice, which developed in designing, that a single mass-spring system can be used unless the loading rate becomes very high. Also the investigations confirm the presumption that especially the shear forces resulting from such a simple design model, should be mistrusted.

10 References

1. Biggs, J. M., Introduction to Structural Dynamics, McGraw-Hill Book company, New York, 1964.
2. Baker, W. E., P. A. Cox, P. S. Westine, J. J. Kulesz and R. A. Strehlow, Explosion Hazards and Evaluation, Elsevier, 1983.
3. Lamb, H., Proceedings of the Royal Society, series A. 93, p. 223–251, 1971.
4. Timoshenko, S., Philosophical Magazine, series 6, 41, p. 744–746, 1921.
5. Leussink, J. W., Response of a dynamically loaded beam, Graduation Report TU Delft, Dept. of Civil Engineering, Delft, 1983 (in Dutch).
6. Heinsbroek, A. G. T. J., Rectangular plates under impact loading; part I: Theory; part II: Working-out and results, Graduation Report, TU Delft, Dept. of Civil Engineering, published by TNO-PML under no. PML 1984-IN-11 and PML 1984-26-IN, Delft, 1984 (in Dutch).
7. Mindlin, R. D., Influence of Rotatory Inertia and Shear on Flexural Motions of Isotropic, Elastic Plates, Journal of Applied Mechanics, March, 1951.
8. Flügge, W. and E. E. Zajac, Bending Impact Waves in Beams, Ingenieur-Archiv, p. 59–70, XXVIII volume 1959.
9. Veen, C. v.d., Explosions in tunnels, Graduation Report, TU Delft, Dept. of Civil Engineering, Delft, 1982 (in Dutch).
10. Willems, P., TILLY, User's Guide, Graduation Report, TU Delft, Dept. of Civil Engineering, Delft, 1985 (in Dutch).
11. Bouwma, A. L., Dynamics of structures, Part 4: Cables and beams, lecture notes b15A, TU Delft, Dept. of Civil Engineering, Delft, 1979 (in Dutch).
12. Structures to resist the effects of accidental explosions, (TM 5-1300, NAVPAC P-397, AFM 88-22), Depts. of the Army, the Navy and the Air Force, June 1969.
13. Harmanny, ir. A., Reinforced Concrete Plates under Static and Dynamic Loading, Proceedings of the International Symposium on Military Applications of Blast Simulation, Oxford GB, September 1985.
14. Mainstone, R. J., The Effect of Impact Loading on Building; Part 4: Properties of Materials at High Rates of Straining or Loading, 21-IL RILEM Committee, Materiaux et Constructions, Vol. 8, No. 44, 1975.
15. Brandes, K., E. Limberger, J. Herter and K. Berner, Kinetic Load Bearing Capacity of Reinforced Concrete Members under Impact Load; Reinforcing Steel Tension Tests with High Strain Rates (in German), Forschungsbericht 129, Bundesanstalt für Materialprüfung, Berlin, 1986.
16. Amman, W., Stahlbeton und Spannbetontragwerke under stossartiger Belastung, Institut für Baustatik und Konstruktion, Zürich, 1982.
17. Amman, W., M. Mühlematter and H. Bachmann, Versuche a Stahlbeton- und Spannbetonbalken unter stossartiger Beanspruchung, Institut für Baustatik und Konstruktion, Zürich, 1982.

18. AMMAN, W., M. MÜHLEMATTER and H. BACHMANN, Versuche a Stahlbeton- und Spannbetonbalken unter stossartiger Beanspruchung, Teil 3: Resultate der Balken P1, P2, B1 bis B8, Institut für Baustatik und Konstruktion, Zürich, 1982.
19. AMMAN, W., M. MÜHLEMATTER, and H. BACHMANN, Versuche a Stahlbeton- und Spannbetonbalken unter stossartiger Beanspruchung, Teil 4: Resultate der Balken B9 bis B21, Institut für Baustatik und Konstruktion, Zürich, 1982.
20. MIER, J. G. M. VAN, e.a., Examples of Non-linear Analysis of Reinforced Concrete Structures with DIANA, HERON, Vol. 32, No. 3, 1987.
21. SLUYS, L. J., Model for cyclic loads at dynamically loaded reinforced concrete beams, Graduation Report, TU Delft, Dept. of Civil Engineering, Delft, 1988 (in Dutch).
22. CUR-report, No. 23, page 27 (in Dutch).
23. ZANTVOORT, P. VAN, Failure of concrete panels under explosion loads, Graduation Report, TU Delft, Dept. of Civil Engineering, Delft, 1988 (in Dutch).
24. KOK, A. W. M., Pulses in Finite Elements, Proceedings of the First International Conference on Numerical Methods in Engineering, New York, 1981.
25. BLAAUWENDRAAD, J. and A. W. M. KOK, Handicraft in Finite Elements, Proceedings of the International Conference on Numerical Methods in Engineering, Swansea, 1987.
26. BLAAUWENDRAAD, J., A. G. T. J. HEINSBROEK and L. J. SLUYS, Discrete Element Method and Beam Dynamics, an Application of TILLY, IABSE Colloquium: Computational Mechanics of Concrete Structures - Advances and Applications, Delft, 1987.
27. BRUIJN, W. A. DE, Reinforced concrete; a new approach. Crack width and stiffness, Graduation Report, TU Delft, Dept. of Civil Engineering, Report 5-85-DR18, Delft, 1985 (in Dutch).
28. BRUGGELING, A. S. W. and W. A. DE BRUIJN, Theory and practice of reinforced concrete, pages 130-134, Stichting Professor Bakkerfonds, Delft, 1986 (in Dutch).
29. BRUIJN, W. A. DE, Theory and practice of reinforced concrete, Book of formulas, pages 23-41, 51-56, TU Delft, Dept. of Civil Engineering, Delft, 1987 (in Dutch).
30. ZIELINSKI, A. J., Fracture of Concrete and Mortar under Uniaxial Impact Tensile loading, Page 5, Thesis, TU Delft, Delft, 1982.
31. BLAAUWENDRAAD, J., TILLY Introduction Manual, TU Delft, Dept. of Civil Engineering, August 1989 (in Dutch).
32. MERKS, P. J. G., TILLY Input/Output Description, TU Delft, Dept. of Civil Engeneering, August 1989 (in Dutch).

Summary

In the current engineering practice the design of impact loaded, physically non-linear structures is usually carried out with the relatively simple single degree-of-freedom system. The question arises whether this model is always adequate. Intuitively, the deformed shape of the structure due to rapidly or locally varying loads is not identical to the deformed shape as a result of static loading conditions.
In this report a model has been developed using discrete mass elements and spring elements, in order to take into account the inertias and deformations necessary to properly describe the behaviour of a beam under transient loading conditions. Because of the probability of relatively short wave phenomena, it has been decided to implement the theory according to Timoshenko in the model. This means that translation and rotation inertia as well as bending and shear deformation are taken into account. As this model is rather new and the problem of elasto-plastic dynamics is not too well known, much attention has been paid to the verification and validation of the computation technique itself.
The density of the geometrical discretisation, which is required to adequately describe the high eigenmodes, was examined. Next, the time step, required to carry out a reliable computation of the eigenperiods of the highest significant eigenmodes, was determined. The solution method used has the property that the errors in the computation of the amplitudes are of a much smaller magnitude than the errors in the periods.
Having obtained enough confidence in the model and the solution method, many computations were carried out, with varying support and loading conditions. The variation in loading conditions concerned the distribution along the beam (uniformly versus concentrated) and the shape and characteristic period of the time function. In this way fields of application for the single degree-of-freedom system were marked out. Some attention was paid to the implementation of the more complicated non-linear behaviour of concrete beams under bending.
The elasto-plastic response for the simply supported beam to a uniform explosion load was computed and evaluated. The value of the plastic bending moment was expressed as a percentage of the maximum bending moment occurring in the linear-elastic case. This percentage varied between 20 and 50. The pure elastio-plastic behaviour was extended with hardening after yielding and its influence on the response was studied. Including hardening had a restricted influence on the maximum deflection, but a tremendous influence on the maximum resulting plastic curvature.
The subsequent stage of the research concerned the simulation of three experiments. It was the objective to support confidence in the model as a tool to predict the damage of real structures. Properties of great interest were the maximum plastic curvature and the remaining permanent curvature. To compute these in a more appropriate way a new type of spring was added to the program. This spring describes cracking and hysteretic effects due to cyclic loading conditions.
In this study the emphasis is on the computation of the response. The value of the model to predict damage and failure is only determined in the last chapter. With the

model failure due to deformations exceeding the rotation capacity of plastic hinges can be predicted. The failure due to shear force was studied less extensively, but with regard to the possible application of the model in this respect, indications are positive.
Designing structures with the single degree-of-freedom mass-spring system is generally only permitted in those cases in which the load duration is not too short and the load distribution not very concentrated. In particular the magnitudes of shear forces and support reactions are not accurately predicted by the simple model.